DOI: 10.1070/RCR4867

Synthesis, properties and applications of semiconductor nanostructured zinc sulfide

Stanislav I. Sadovnikov

Institute of Solid State Chemistry, Ural Branch of the Russian Academy of Sciences, ul. Pervomaiskaya 91, 620990 Ekaterinburg, Russian Federation

Experimental results obtained in recent years on the synthesis, structure and properties of nanostructured zinc sulfide are summarized and analyzed. The crystal polymorphs of zinc sulfide and methods for the synthesis of zinc sulfide as quantum dots, nanospheres, doped nanoparticles, thin films and heteronanostructures with different morphology are described. The attention is focused on the emission and semiconductor properties of the title compound. The potential applications of zinc sulfide-based nanostructures are considered.
The bibliography includes 194 references.

Contents

1. Introduction 571
2. Structure and semiconductor characteristics of zinc sulfide 572
3. Methods for the synthesis of nanostructured zinc sulfide 574
4. Control of morphology of zinc sulfide nanostructures 583
5. Properties and application of nanostructured zinc sulfide 585
6. Conclusion 589

1. Introduction

The modern scientific and technological progress is based on electronics, computer and biomedical technologies and nanotechnologies. In the last decade, nanomaterials and nanotechnologies based on semiconductor sulfides have been investigated especially actively. The efforts of researchers in these fields are concentrated on the development of synthetic routes towards nanostructured materials with controlled dimensional and morphological characteristics and electronic and optical properties.

Zinc sulfide (ZnS) is among the first discovered semiconductors. The luminescence of zinc sulfide, which was detected experimentally back in 1866,[1] was initially used for scientific research and later for practical purposes. In particular, in experiments on the scattering of charged particles by the nuclei of various elements carried out in 1907 – 1911, E.Rutherford used a zinc sulfide-coated screen as a scintillation detector. Studies of the semiconductor properties of zinc sulfide started in the 1920s – 1930s and were actively developed in the mid-20th century, being related to ZnS polymorphism.[2] Currently, this research is still in progress.[3] Difficulties involved in the studies of ZnS luminescence and dependence of luminescence on doping have been considered.[4]

Like lead,[5,6] silver,[7–12] copper,[13] cadmium[14] and mercury[15] sulfides, zinc sulfide is a highly demanded compound:[16,17] it is used in ultrasound amplifiers and detectors, infrared sensors, and near- and middle-IR lasers.[18] Coarse-crystalline zinc sulfide is employed most widely as a luminophore for the design of low- and high-voltage cathodoluminophores, photoluminophores and other luminescent devices,[19] light emitting diodes and liquid-crystal displays.[20]

Currently, the energy demand of the mankind is largely provided by combustion of fossil energy sources — oil, gas and coal. A promising trend that should reduce the consumption of these natural resourses is the conversion of solar energy to electricity. The engineering devices that accomplish this conversion are solar batteries, the fabrication of which requires ZnS.

Zinc sulfide has a broad transmission band, ranging from visible light with a 0.4 μm wavelength to IR light with a 16 μm wavelength;[21] therefore, it is used to manufacture parts of optical instruments and devices.

Zinc sulfide nanostructures emit in the UV and visible regions. The functional emission properties of ZnS nanostructures and their use as emitters are directly related to the morphology of these nanostructures, as follows from the basic relationships describing the emission.

Field (or autoelectronic) emission is the emission of electrons by a solid under the action of a rather strong external electric field. According to the Fowler – Nordheim law, the emission current (I) is described by the equation

S.I.Sadovnikov. Candidate of Chemical Sciences, Senior Researcher of the Laboratory of Non-stoichiometric Compounds of the ISSC UB RAS. Telephone: +7(343) 362 – 3034, e-mail: sadovnikov@ihim.uran.ru
Current research interests: synthesis, structure and reactivity of metal chalcogenides, colloid solutions, nanoparticles, nanostructured materials.

Received 11 October 2018
Translation: Z.P.Svitanko

© 2019 Uspekhi Khimii, Russian Academy of Sciences and Turpion Ltd.

$$I = S\frac{A\beta^2 E^2}{\phi}\exp\left(-\frac{B\phi^{3/2}}{\beta E}\right) \quad (1)$$

where A and B are constants, S is the surface area of the emitter, ϕ is the work function potential of the emitter material, $\beta \approx h/r$ is the enhancement factor, which depends on the emitter geometry (h and r are the length and the curvature radius of the emitter tip), $E = V/d$ is the local electric field strength, V is the applied potential and d is the distance between the emitter and the anode.

The key factors determining the emission current include the work function $\Phi = e\phi$ of the emitting material (e is the electron charge), the local electric field strength, the distance between the emitter and the anode and the emitter geometry. The work function for the coarse-crystalline zinc sulfide is 7 eV. Once the electric field strength E is set, a material with lower potential ϕ, or lower work function Φ can generate a higher emission current. The enhancement factor and, hence, the emission current can be increased by increasing the aspect ratio h/r or by decorating the nanostructure surface by metal nanoparticles with a low work function (*e.g.*, platinum or silver nanoparticles).[22, 23] From relation (1), it follows that enhanced emission characteristics and luminescent properties among ZnS nanostructures should be inherent in nanobelts, nanowires and nanotubes and also nanocombs and nanoribbon and nanowire arrays.[24]

The large number of scientific publications addressing metal sulfides attests to enhanced researchers' attention to such compounds. More than one and a half thousand original papers published after the year of 2000 deal with the synthesis and properties of nanocrystalline ZnS alone. Some reviews consider the studies of lead, cadmium and silver sulfides.[5–7, 14] However, survey publications on nanostructured ZnS are scarce; a brief mention of ZnS nanoparticles is present only in one review[25] devoted to semiconductor nanoparticles with spatial charge separation; one more review[16] addresses the properties and applications of zinc sulfide nanostructures for solar cells, and a brief review[17] deals with doped ZnS thin films.

However, no survey publications on nanostructured zinc sulfide are still present in the Russian literature. This review was intended to fill this gap.

The following designations are used:

a_B — Bohr radius,
A, B — constants,
β — enhancement factor,
d — distance between the emitter and the anode,
E — local electric field strength,
E_g — band gap,
ε_{11}, ε_{33} — dielectric constants,
ϕ — work function potential,
FCC — face-centred cubic,
h — emitter tip length,
$\hbar$ — Planck's constant,
hkl — Miller indices,
HRTEM — high resolution transmission electron microscopy,
I — emission current,
IP — ionic product,
K_{sp} — solubility product,
m_{ex} — exciton mass,
m_e — effective electron mass,
m_h — effective hole mass,
m_0 — free electron rest mass,
μ_{ex} — reduced exciton mass,
PEG — polyethylene glycol,
QD — quantum dot,
r — emitter radius of curvature,
R_{ex} — characteristic exciton size,
S — emitter surface area,
S_s — solution supersaturation,
SEM — scanning electron microscopy,
SILAR —successive ionic layer adsorption and reaction,
TEM — transmission electron microscopy,
TNT — 2,4,6-trinitotoluene,
TOPO — trioctylphosphine oxide.

2. Structure and semiconductor characteristics of zinc sulfide

Zinc sulfide is the only compound formed in the Zn – S system; it contains ~50 at.% of sulfur and has a melting point of 1991 K.[26]

The low-temperature cubic polymorph α-ZnS (space group $F\bar{4}3m$) possessing semiconductor properties has a zinc blende or sphalerite structure ($B3$ type) and is stable at $T < 1290$ K; at $T = 1293$ K, it transforms into the high-temperature hexagonal polymorph β-ZnS (space group $P6_3mc$) with the wurtzite structure ($B4$ type), which retains the semiconductor properties.[26]

At 300 K, cubic α-ZnS has the lattice constant $a = 0.54109$ nm.[27] According to X-ray diffraction data, the unit cell of β-ZnS has $a = 0.38230$ and $c = 0.62565$ nm;[28] according to neutron diffraction data,[29] $a = 0.38227$ and $c = 0.62607$ nm. The zinc and sulfur atomic coordinates in the unit cells of zinc sulfide polymorphs are summarized in Table 1.

The crystal structures of α- and β-ZnS are composed of successively alternating close-packed atoms (ions) of different sorts shifted relative to one another (Fig. 1).

The structure of α-ZnS represents a cubic close packing (Fig. 1 *a*). In this structure, the Zn and S atoms occupy the same points as in the diamond structure, but in an ordered fashion; therefore, the lattice is split into two non-equivalent face-centred cubic (FCC) sublattices with four points in each. The FCC sublattices are shifted relative to each other in the $[1/4\ 1/4\ 1/4]_{B3}$ direction.

The structure of β-ZnS is a hexagonal close packing in which layers are arranged perpendicular to the $[001]_{B4}$ direction (Fig. 1 *b*). In the ideal wurtzite structure, the basis of the lattice contains two metal atoms in 2(*b*) sites with the coordinates (1/3 2/3 0) and (2/3 1/3 1/2) and two non-metal atoms in 2(*b*) sites with the coordinates (1/3 2/3 3/8) and (2/3 1/3 7/8). In the real β-ZnS structure, the sulfur atoms are somewhat shifted along the z coordinate (see Table 1).

The structures of α and β polymorphs of coarse-crystalline zinc sulfide differ in the sequence of layer alternation. If the lower layer is designated by A, then the ABC sequence of layers occurs in a cubic sphalerite type structure (see Fig. 1 *a*) and the AB sequence is present in the hexagonal wurtzite structure (see Fig. 1 *b*). The two structures have the same atomic densities.

In the coarse-crystalline sphalerite and wurtzite structures, each atom is located in the tetrahedral environment of four atoms of another sort. According to Wright *et al.*,[30] in the cubic sphalerite, the lowest surface energy of 0.65 J m^{-2}

Table 1. Crystal structure parameters of the low- and high-temperature zinc sulfide polymorphs at 298 K.[27, 29]

Crystal system, structural type, space group	Unit cell parameters /nm	Atom	Site and multiplicity	Atomic coordinates [a]			Point occupancy
				x/*a*	*y*/*b*	*z*/*c*	
Low-temperature polymorph α-ZnS							
Cubic, *B*3 type, $F\bar{4}3m$ (T_d^2)	a = 0.54109	Zn	4(*a*)	0	0	0	1
		S	4(*b*)	0.25	0.25	0.25	1
High-temperature polymorph β-ZnS							
Hexagonal, *B*4 type, $P6_3mc$ (C_{6v}^4)	a = 0.38227, c = 0.62607	Zn	2(*b*)	1/3	2/3	0	1
		S	2(*b*)	1/3	2/3	0.3748	1

[a] *x*, *y*, *z* are coordinates; *a*, *b*, *c* are unit cell parameters.

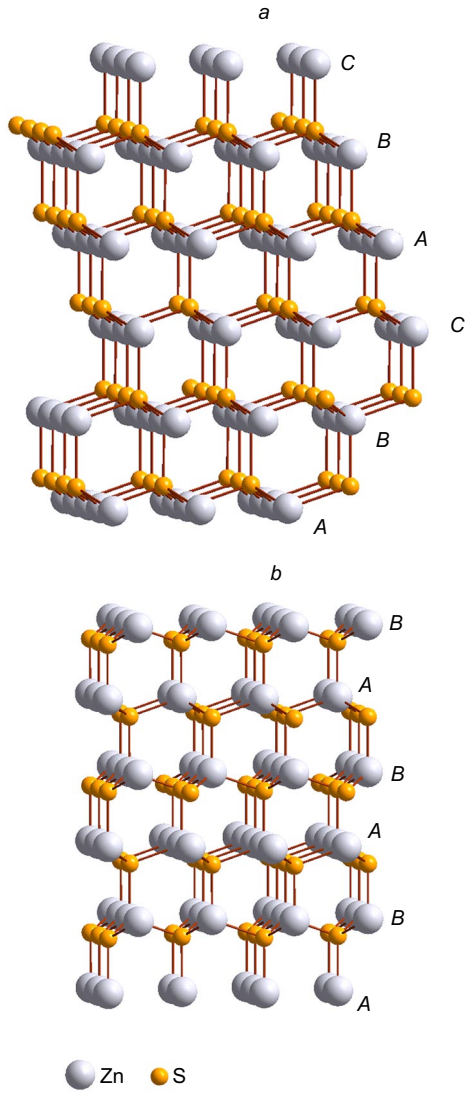


Figure 1. Crystal structures of cubic sphalerite (*a*) and hexagonal wurtzite (*b*) type ZnS.

is inherent in the electrically neutral (110) plane containing equal numbers of zinc and sulfur atoms (ions). For comparison, the energies of the (001) planes formed by only zinc or only sulfur atoms are two times higher, being 1.31 and 1.25 J m^{-2}, respectively. The energies of the (111) planes also formed by either zinc atoms or sulfur atoms alone are somewhat lower, being 1.03 and 1.12 J m^{-2}. It was shown [31] that the distribution of atoms on the (110) surface of sphalerite is distorted: the sulfur atoms occur in the prismatic environment, while the zinc atoms retain the tetrahedral environment formed by sulfur atoms.

The (1010) and (1120) surface energies of β-ZnS were found [32] to be 0.51 and 0.32 J m^{-2}, respectively, which is noticeably lower than these values for crystallographic planes of α-ZnS. An important feature of β-ZnS is the presence of polar surfaces.[33] The (0001) plane is the most frequently encountered polar surface.† Positively charged zinc ions give rise to positively charged (0001) surfaces, while sulfur atoms generate negatively charged (000 – 1) surfaces. The opposite charges of the polar surfaces result in spontaneous polarization along the *c* axis. The anisotropic growth of the wurtzite type ZnS is driven by different surface energies of crystallographic planes and their polarity; furthermore, the surfaces formed by zinc atoms are chemically reactive, with nanostructures readily growing on them, while the surface formed by sulfur atoms is relatively inert.

For wurtzite, it was found [34] that the (001) surface has the maximum energy (0.91 – 1.52 J m^{-2}), the (110) surface has the minimum energy (0.28 – 0.49 J m^{-2}), and the (100) surface has an intermediate energy (0.52 – 1.0 J m^{-2}). In sphalerite, the highest energies are inherent in the (111) and (100) faces; the surface energies of other faces are < 1.0 J m^{-2} (Ref. 34), which is in line with the results of Wright *et al.*[30] The average surface energy of three-dimensional spherical sphalerite nanoparticles (0.79 J m^{-2}) exceeds the average surface energy of analogous wurtzite particles (0.57 J m^{-2}).

The surface energy of ZnS nanoparticles depends on the number of broken bonds and slowly declines as this number decreases.[35] Khalkhali *et al.*[36] found that ZnS nanoparticles of > 3 nm size with the initial wurtzite or sphalerite crystal structure are composed of a crystalline core surrounded by a distorted network of tetrahedrally coordinated atoms, which form four- and six-membered rings, and of a surface mainly formed by three-coordinate atoms. As the nano-

† The four-digit hexagonal indices *hkil* are equivalent to three-digit indices *hkl*, as $i = -h - l$; therefore, for example, the [0001] and [001] directions used by different authors to describe hexagonal structures imply one and the same direction along the *c* axis.

particle size decreases to 2 nm, the crystalline core disappears and all atoms become three-coordinate.

Under normal conditions, the coarse-crystalline zinc sulfide is a direct-gap semiconductor. The band gap (E_g) of cubic α-ZnS at 300 K is ~3.54 – 3.76 eV,[37,38] while that of hexagonal β-ZnS is ~3.74 – 3.91 eV.[17,37–39] The E_g value for ZnS depends on temperature: for cubic and hexagonal zinc sulfide, the dE_g/dT derivatives are -4.7×10^{-4} and -3.0×10^{-4} eV K^{-1}, respectively.[38]

For coarse-crystalline hexagonal ZnS at 300 K, the effective masses of an electron and a hole are $m_e = 0.28\,m_0$ and $m_h = 0.49\,m_0$,[38] where $m_0 = 9.1 \times 10^{-31}$ kg is the rest mass of a free electron. Therefore, the reduced mass of the exciton

$$\mu_{ex} = \frac{m_e m_h}{m_e + m_h} \quad (2)$$

is $\sim 0.18 m_0 = 1.62 \times 10^{-31}$ kg for hexagonal ZnS.

The characteristic size of the Wannier – Mott exciton in the macroscopic semiconductor crystal is

$$R_{ex} \approx \frac{n^2\hbar^2\varepsilon}{\mu_{ex}e^2} = \frac{n^2\varepsilon m_0}{\mu_{ex}} a_B \quad (3)$$

where n is the exciton state, $a_B = \hbar^2/m_0e^2 = 0.0529$ nm is the Bohr radius. The dielectric constant values found for hexagonal zinc sulfide at 300 K were $\varepsilon_{11} = \varepsilon_{33} = 8.7$,[38–40] $\varepsilon_{11} = 8.1$ and $\varepsilon_{33} = 8.5$ (Ref. 41) or $\varepsilon_{11} = 8.31$ and $\varepsilon_{33} = 8.76$.[42] According to a reference book,[38] the dielectric constants of cubic and hexagonal zinc sulfide are 8.9 and 8.75, respectively. If the exciton reduced mass $\mu_{ex} = 0.18\,m_0$ and the dielectric constant for ZnS is in the range from 8.1 to 8.76, then for coarse-crystalline zinc sulfide, the size of the first exciton state with $n = 1$ is $R_{ex} \sim 2.4 – 2.6$ nm.

3. Methods for the synthesis of nanostructured zinc sulfide

Zinc sulfide, which is highly chemically stable and has low solubility, wide band gap, wide transmission range (from visible to IR region) and unique luminescent and optical properties, is utilized for the synthesis of nanocrystals, quantum dots, nanostructured films, core/shell structures, isolated nanoparticles and other nanostructures.

The key types of nanomaterials, as regards the dimensionality and morphology, are zero- (0D), one- (1D), two- (2D) and three-dimensional (3D) ones.[43–45] Zero-dimensional nanomaterials are quantum dots (QD) and isolated nanoparticles; one-dimensional nanomaterials include nanofibrous and nanotubular materials such as quantum wires (the length of fibres, rods or tubes with a diameter of 5 – 40 nm varies from 100 nm to tens of μm); two-dimensional materials are nanometre-thick films and semiconductor nanoheterostructures such as quantum wells (nanoparticles of different dimensionality may occur in a liquid or solid matrix or on a substrate); three-dimensional materials are powders and fibrous, multilayer and polycrystalline materials in which 0D, 1D or 2D particles tightly adjoin one another, giving rise to interfaces.

Zinc sulfide nanostructures such as ZnS-based nanopowders, quantum dots and other nanostructures are prepared by various methods: chemical bath deposition from aqueous and alcohol solutions; sol – gel methods; microemulsion synthesis; thermolysis; template, sonochemical, and hydro- and solvothermal syntheses; electrochemical, microwave and other methods. Each method has its own benefits and drawbacks. Among the drawbacks, note, first, the fact that many methods are not universal and may give nanostructured zinc sulfide only in one form (*e.g.*, as quantum dots, nanopowders or films), second, insufficient control of the nanoparticle size during the synthesis (resulting in broad particle size distribution of the nanomaterials), and also the use of multistep (3 – 4 steps) processes, complex equipment and special protection means, elevated temperatures and rare, expensive and hazardous reagents.

Nano-sized particles are unstable, as high surface energy promotes their aggregation. The generation of a shell of organic ligands on the nanoparticles prevents particle aggregation and growth as well as their oxidation, thus providing the formation of stable isolated nanoparticles. Using a protective shell, it is possible to control the sizes of isolated nanoparticles.

Most of nanomaterials are thermodynamically non-equilibrium. The diverse morphology of nanoparticles reflects the metastability, *i.e.*, the occurrence of the system in a particular local free energy minimum.[42,45]

3.1. Quantum dots and nanospheres

Stable ZnS quantum dots were first synthesized by Rosetti *et al.*[46] The reaction of $Zn(ClO_4)_2$ and Na_2S was conducted in methanol solutions. Joo *et al.*[47] obtained cubic ZnS nanocrystals with ~11 nm size by reacting $ZnCl_2$ with sulfur in oleylamine at elevated temperature in the presence of trioctylphosphine oxide (TOPO). Zhao *et al.*[48] synthesized hexagonal ZnS nanocrystals with an average size of ~4 nm (Fig. 2); the starting reactants, $ZnCl_2$ and thiourea, were allowed to react in ethylene glycol at ~420 K.

Cubic ZnS nanoparticles with the size of ~15 to ~30 nm were obtained by the hydrothermal process in aqueous solutions of zinc sulfate and sodium sulfide without coating agents.[49] The synthesis was carried out in an autoclave at 490 K for 12 h.[47] Bodo and Singh[50] prepared 6 – 10 nm ZnS quantum dots with a cubic structure in an alkaline medium with pH 9 – 11; the reaction mixture contained zinc sulfate, thiourea and ammonium hydroxide; a

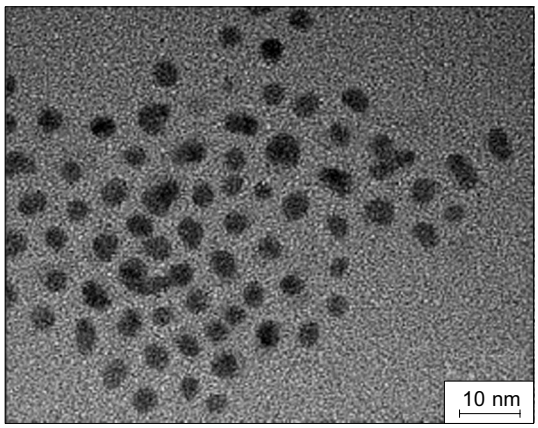


Figure 2. Transmission electron microscopic (TEM) image of ZnS quantum dots with an average size of ~4 nm synthesized in ethylene glycol at ~420 K.[48]

3% solution of polyvinyl alcohol served as the coating agent.

The attention of researchers is attracted by hollow nanospheres, which have a very low density and high specific surface area. Owing to these features, ZnS hollow nanospheres are used in catalysis and nanoelectronics, for the development of lightweight structural materials and drug delivery systems.[51 – 54] For the preparation of ZnS hollow nanospheres, SiO_2 or polystyrene microspheres are usually employed as templates;[55, 56] however, the size of the resulting nanospheres is >100 nm. A simple process for the fabrication of ZnS hollow nanospheres without using templates has been reported.[57] The synthesis was carried out by a hydrothermal method in an autoclave at 410 K for 5 h using an aqueous thiourea and zinc acetate mixture. According to X-ray diffraction data, ZnS hollow nanospheres had a hexagonal wurtzite structure. An image of ZnS nanospheres pretreated with a dilute HCl solution to decrease the shell thickness is shown in Fig 3 *a*. The size of the hollow nanospheres varied in the range from 200 to 300 nm, with the average shell thickness being $\sim$20 nm.

One more process for the synthesis of ZnS hollow nanospheres with a diameter of <100 nm has been proposed (Fig. 3 *b*).[58] The synthesis was carried out in an aqueous solution containing the P123 triblock copolymer, zinc acetate and thioacetamide at 300 K for 10 h. The diameter of the ZnS hollow nanospheres thus formed was 50 – 70 nm, while the shell thickness was $\sim$15 nm. The ZnS nanocrystals forming these nanospheres were cubic.

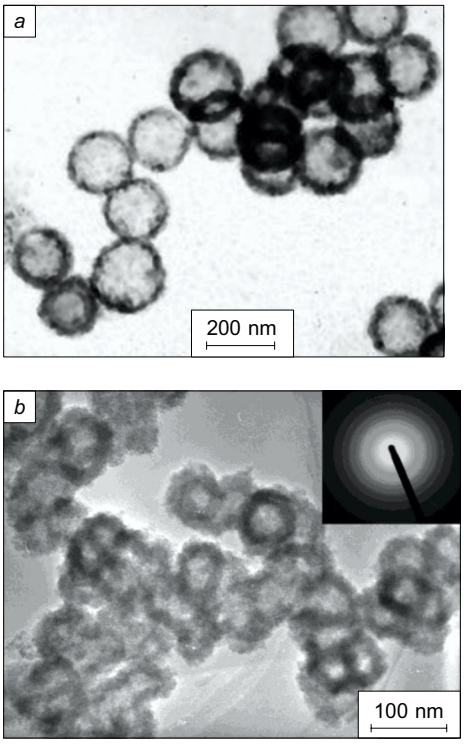


Figure 3. TEM images of ZnS hollow nanospheres.
(*a*) Hydrothermal synthesis from a mixture of thiourea and zinc acetate in an autoclave at 410 K for 5 h;[57]
(*b*) synthesis in an aqueous reaction mixture containing the P123 triblock copolymer, zinc acetate and thioacetamide at 300 K for 10 h.[58]

Gu *et al.*[59] obtained ZnS hollow microspheres in aqueous solutions of $Zn(NO_3)_2$ and thioacetamide without surface modification. A hydrothermal process involving $Zn(NO_3)_2$, thioacetamide and polyethylene glycol (PEG) was reported.[60] The size of ZnS hollow microspheres appreciably depended on the PEG chain length. Microspheres with a $\sim$0.2 μm size were formed without PEG; in the presence of PEG-800, PEG-2000 and PEG-6000, microspheres with an average size of $\sim$2, $\sim$4 and $\sim$5 μm, respectively, were obtained.

Solid ZnS nanospheres assembled from cubic ZnS nanosheets were synthesized by the hydrothermal process at 470 K in an aqueous solution of $Zn(NO_3)_2$ and L-cysteine as the source of sulfur.[61] The solvothermal synthesis of ZnS nanospheres was accomplished at 470 K using solutions of $Zn(NO_3)_2$ and L-cysteine containing ethanolamine or ethylenediamine. When ethanolamine was added, the nanospheres were assembled from ZnS nanorods, while the addition of ethylenediamine resulted in nanosphere formation from cubic and hexagonal ZnS nanocrystals of different morphology.[61] This is exemplified in Fig. 4, which shows a TEM image of a ZnS nanosphere consisting of hexagonal zinc sulfide nanorods.

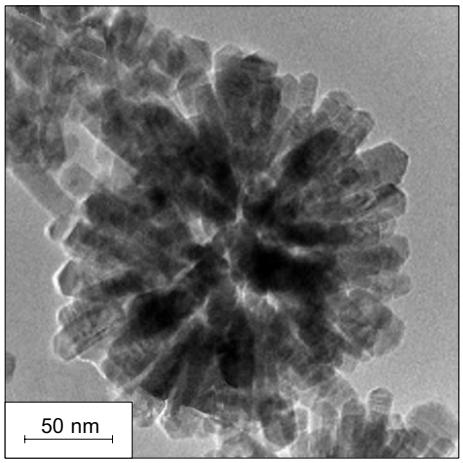


Figure 4. TEM image of a ZnS nanosphere assembled from zinc sulfide nanorods.[61]

Core/shell type quantum dots are synthesized in order to enhance their quantum efficiency. In this type of quantum dots, ZnS usually serves as the shell material. Talapin *et al.*[62] were the first to report the fabrication of CdSe/ZnS nanoparticles with a high photoluminescence quantum yield, reaching 50% – 60%. These nanoparticles were synthesized in several stages. First, monodispersed CdSe nanocrystals with a photoluminescence quantum yield of 10% – 25%, which decreased with increasing particle size, were prepared in a hexadecylamine – trioctylphosphine oxide – trioctylphosphine three-component system. Then the ZnS shell was grown on the surface of CdSe nanocrystals. The maximum photoluminescence quantum yield, equal to 66%, was observed when the core was 1.6 monolayers thick. Xie *et al.*[63] gradually changed the shell composition in the radial direction (from CdS to ZnS) using the successive ionic layer adsorption and reaction (SILAR) method. The quantum dots with a multilayer shell of variable composi-

tion showed an even higher photoluminescence quantum yield.

The benefits of the multilayer-shell quantum dots were utilized [64] to fabricate a CdTe/CdSe/ZnS heteronanostructure with an average core diameter of 2.6 nm, which showed a high photoluminescence quantum yield (84% in aqueous media). The average diameters of CdTe/CdSe core/shell type quantum dots were 3.2, 4.0, 4.8 and 5.5 nm for one-, two-, three- and four-layer CdSe shells, respectively. The size of the CdTe/CdSe/ZnS quantum dots in which the six-layer shell was composed of four CdSe layers and two ZnS layers reached 6.7 nm. The additional ZnS shell efficiently restricted the electron and hole migration in the CdTe/CdSe structure and substantially improved their indirect recombination on the CdTe core and the CdSe shell inner surface. In the opinion of some researchers (*e.g.*, Ref. 16), the fabrication of highly luminescent CdTe/CdSe/ZnS heteronanostructure with an emission wavelength from 540 to 826 nm is among the best achievements in the development of luminescent semiconductor nanocrystals.

Most of the above methods for the synthesis of ZnS nanocrystals, quantum dots and nanospheres are based on hydro- and solvothermal processes at a temperature of 400 – 500 K and employ TOPO and L-cysteine as stabilizing and coating agents, with L-cysteine being also able to act as a source of sulfur. Nanocrystals with a hexagonal structure are synthesized in solutions with a low TOPO concentration; a higher TOPO content and alkaline medium stabilize the cubic structure of ZnS nanocrystals.

3.2. ZnS nanostructures with various morphology

One-dimensional nanostructures such as nanowires, nanofibres, nanothreads, nanotubes, nanorods, nanobelts, nanoribbons, nanocombs, as well as nanostructures of higher dimensionality composed of one-dimensional components attract attention for their potential engineering applications. Methods used to prepare one-, two- and three-dimensional ZnS nanostructures are commonly high-temperature chemical processes.

The best known one-dimensional nanostructures are nanowires, nanotubes and nanorods. Among all of them, nanowires have the highest aspect ratio and are fairly flexible. Nanorods, which may have either a round or hexagonal cross-section, are substantially shorter. Nanowires and nanorods are solid, whereas nanotubes are hollow.

The ZnS nanowires, nanorods and other nanostructures are mainly obtained by gas-phase and hydro- or solvothermal syntheses. The solvents commonly used in the solvothermal synthesis include alcohols, benzene, polyamines or hydrazine. The gas-phase synthesis may be implemented as thermal evaporation, chemical vapour deposition, molecular beam epitaxy and laser ablation.

Zinc sulfide nanowires and their arrays with enhanced emission properties were obtained by thermal evaporation of a zinc foil and sulfur under argon at 670 – 700 K with deposition onto the same foil.[65] Several tens of micrometres long ZnS nanowires with a diameter of 30 – 60 nm were synthesized by thermal evaporation of a ZnS powder at 1170 K with a gold film as a catalyst.[66] Electron microscopic and diffraction studies demonstrated that these nanowires are single crystals growing along the [110] crystallographic direction. Barrelet *et al.*[67] subjected the molecular precursor, zinc diethyldithiocarbamate, to thermal decomposition catalyzed by gold nanoclusters. The single crystals of the resulting ZnS nanowires grew along the [100] direction.

Nanorods and nanowires can be fabricated by orientational transformation of the shape of small nanocrystals. For example, Pacholski *et al.*[68] produced ZnO nanorods by a repeated treatment of ZnO nanospheres in a methanol solution. Anisotropic ZnS nanorods with an average size of 5×21 nm and a cubic structure were also obtained by an oriented transformation, using hydrothermal synthesis from a solution containing diethylzinc, sulfur and hexadecylamine at 400 K followed by ageing at 570 K and secondary ageing of the resulting 5 nm ZnS nanospheres in a solution in oleylamine at 230 K for 24 h.[69] The ageing of ZnS nanospheres in a hexadecylamine solution was accompanied by isotropic growth of ZnS nanospheres from 5 to 10 nm.

Ordered arrays of single crystalline ZnS nanowires with controlled orientation are required for nanoelectronics. A typical scanning electron microscopy (SEM) image of a ZnS nanowire array epitaxially grown on the Zn_3P_2 substrate is shown in Fig. 5. All $\sim$500 nm-long nanowires are aligned in the same crystallographic direction and have similar diameters. A characteristic feature of most of the grown nanowires is their smaller diameter at the bottom (near the substrate) and a greater diameter at the top.

Li *et al.*[71] obtained ZnS nanorods by thermolysis of zinc ethyl xanthate dissolved in octylamine, with hexadecylamine being used as a stabilizing ligand.

The synthesis of ZnS nanotubes by the reaction of H_2S with ZnO nanobelts as templates was reported by Wang *et al.*[72] Zinc sulfide nanotubes had a cubic structure and high porosity and consisted of $\sim$7 nm ZnS nanocrystallites. Yin *et al.*[73] proposed a thermochemical process for the fabrication of well-faceted ZnS nanotubes with a hexagonal cross-section by heating a ZnS powder in a graphite crucible in a water vapour atmosphere. Several micrometres long nanotubes with a hexagonal cross-section grew along the [0001] direction; their outer diameter was 100 – 120 nm and the nanotube walls were $\sim$10 nm thick.

The method for the preparation of a ZnS nanotube array reported by Huang *et al.*[74] was as follows. First, a cubic zinc sulfide shell was deposited *via* thermal evaporation on hexagonal ZnO nanorods with a wurtzite structure to give coaxial ZnO/ZnS heterostructures. Then the inner

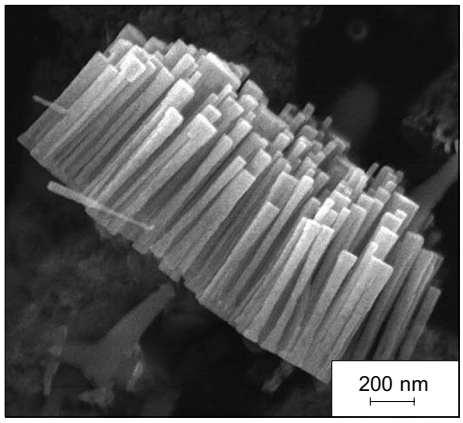


Figure 5. SEM image of a ZnS nanowire array epitaxially grown on the Zn_3P_2 substrate.[70]

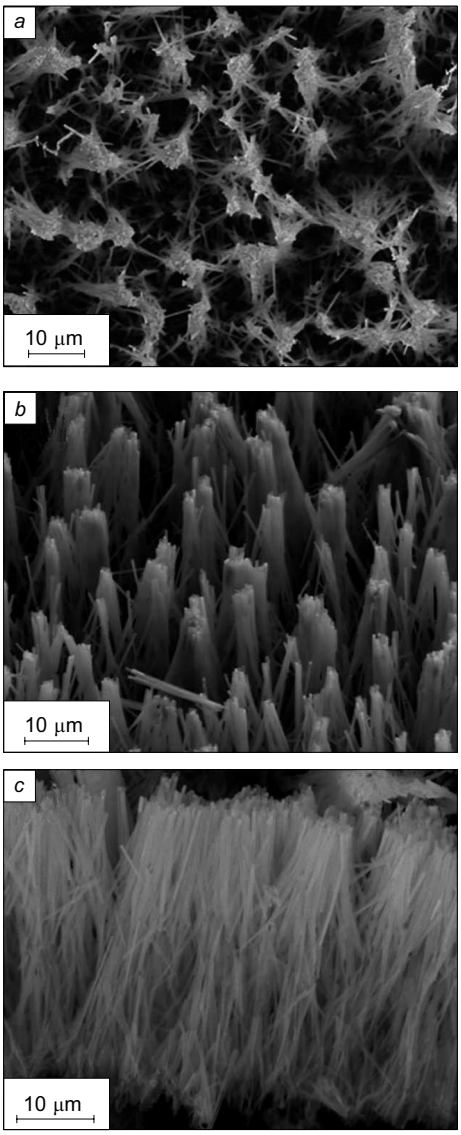


Figure 6. SEM images of a ZnS nanotube array: top view (*a*) and side view (*b*, *c*).[74]

ZnO core of the heterostructure was etched away with an acid to generate ZnS hollow nanotubes oriented along the [002] direction (Fig. 6). The nanotube diameter was ~300 nm and their length reached 30 μm. Thus, the ZnS nanotube array was fabricated by converting an array of ZnO nanorods to an array of ZnO/ZnS nanocables followed by removal of the ZnO core (Fig. 7).

Worthy of note are ZnS nanoribbons and nanobelts, which have a rectangular cross-section, as opposed to nanotubes, nanowires or nanorods. Fang *et al.*[75] synthesized ZnS nanobelts by chemical vapour deposition. A ZnS powder used for the synthesis was evaporated in high-purity argon at 1370 K.

Jiang *et al.*[76] prepared ZnS nanoribbons by thermal evaporation of sphalerite in a quartz tubular furnace at 1370 K in a mixture of high-purity argon with 5% hydrogen. The nanoribbons had a hexagonal structure, a typical length from several tens to several hundred micrometres, a 200 to 400 nm width and a thickness ranging from 1/15 to 1/

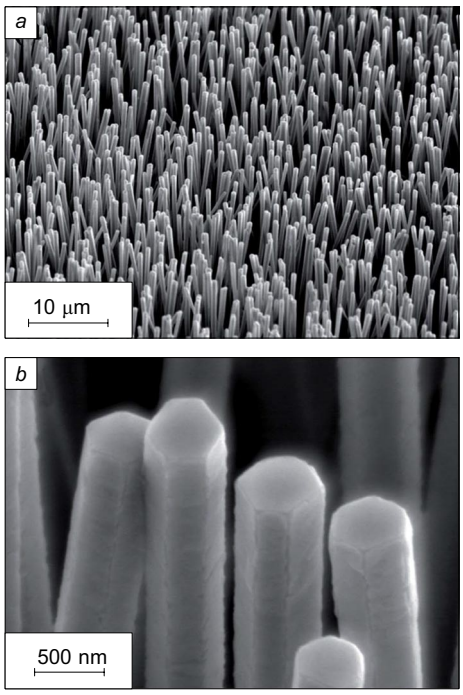


Figure 7. SEM images (side view) of a ZnO/ZnS nanocable array at a low (*a*) and high (*b*) magnification.[74]

20 of the width (~10 to ~30 nm). The nanoribbon width and length depended on the reaction temperature and time, while the thickness was insensitive to the growth conditions. According to the views of Jiang *et al.*,[76] the evaporation of cubic (c) ZnS and formation of hexagonal (h) ZnS can be represented as follows: the cubic ZnS powder reacts with hydrogen at a high temperature to give gaseous zinc and hydrogen sulfide, which are carried to the less heated area of the furnace where they react with each other thus giving hexagonal wurtzite type ZnS.

$$ZnS(c) + H_2 \xrightarrow{1270\,K} Zn\uparrow + H_2S \quad (4)$$

$$Zn\uparrow + H_2S \xrightarrow{1170\,K} ZnS(h) + H_2 \quad (5)$$

The products of reaction (4) migrate along the axis of the quartz tube owing to the temperature gradient, which provides the driving force for the growth of ZnS nanoribbons.

The deposition of a vapourized mixture of ZnS and carbon powders onto a gold film under argon at 1170 K gave rise to single-crystalline several millimetre long ZnS nanobelts (Fig. 8).[77] Thin ZnS nanobelts of ~20 nm thickness were prepared [78] by chemical vapour deposition carried out under argon for 1 h at 1370 K, with ZnS and sulfur powders and carbon nanopowder being used as the reactants.

Aligned arrays of ZnS nanobelts with enhanced field emission were synthesized by thermal evaporation of pressed zinc sulfide nanopowder in an argon atmosphere at a temperature of 1370 – 1420 K without using a template or a catalyst.[79] Lu *et al.*[80] obtained arrays composed of 30 nm thick and ~200 nm wide ZnS nanobelts with a hexagonal structure, which had identical length of up to 4 μm, by the solvothermal reaction of zinc acetate, thiourea

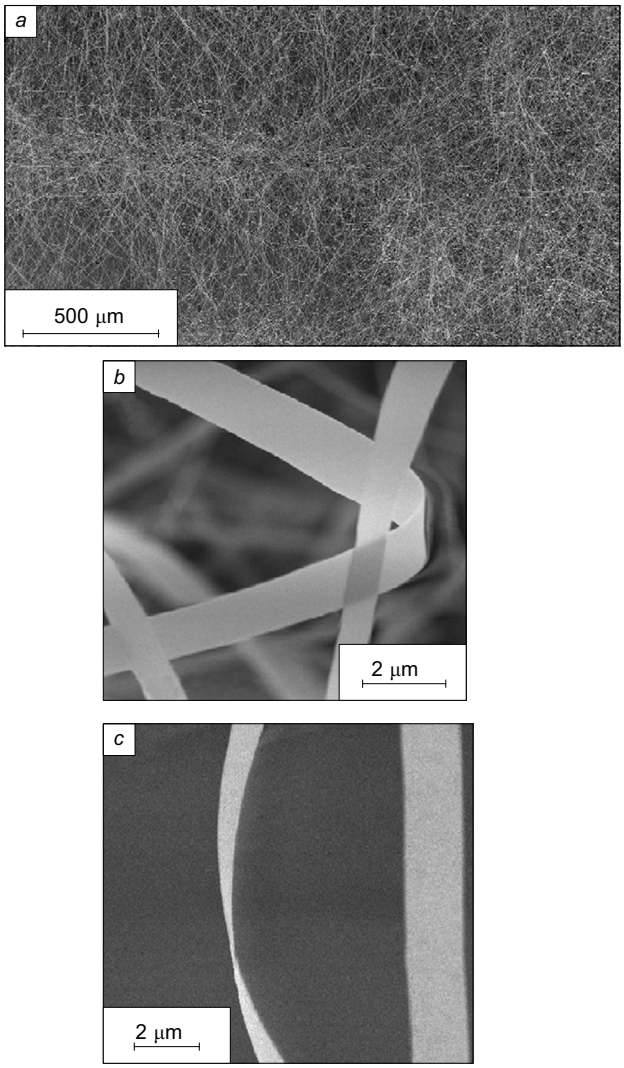


Figure 8. Electron micrograph of ~1 mm long ZnS nanobelts (*a*) and SEM images of <60 nm thick ZnS nanobelts (*b*, *c*).[77]

and ethylenediamine in an autoclave at 430 K. The deposition was performed on a zinc foil, and after that, the foil with the deposited ZnS was subjected to vacuum annealing at 520 K for 30 min. The use of zinc foil as the substrate is the critical factor for the synthesis of the nanobelt array.[80]

One-dimensional ZnS nanostructures, including nanorods and nanowires, and tetrapods as combinations of one-dimensional ZnS nanostructures were synthesized[21] using radiofrequency thermal plasma. The reactant feed and cooling flow rates were the critical parameters of the synthesis determining the morphology of the final products. The synthesis was carried out in a 30 kW radiofrequency thermal plasma reactor. An argon plasma was generated by a water-cooled induction coil with a power supply system operating at 4 MHz frequency; the argon flow rate was 1 $m^3\ h^{-1}$. The reactant mixture of zinc and sulfur powders was continuously injected into the plasma with a carrier gas (nitrogen). The pressure in the reactor chamber was equal to atmospheric. Zinc and sulfur were evaporated, ionized and reacted to give the final product, which was collected on the bottom of the chamber.

In order to study the influence of experimental parameters on the morphology of the final products, the synthesis was carried out at different reactant flow rates and cooling regimes. Depending on the zinc and sulfur feed rate and on whether or not a cooling gas was used, different ZnS nanostructures were formed. When the zinc and sulfur feed rate was 12 g min^{-1}, tetrapods were obtained. The tetrapod legs were up to 200 nm long and up to 80 nm in diameter. When the feed rate was increased to 24 g min^{-1}, nanorods with a length of several micrometres and a diameter of ~80 nm were formed. Further increase in the zinc and sulfur feed rate did not provide the synthesis of uniform tetrapods or nanorods. Nanobelts with ~50 nm width and different lengths (ranging from several tens to a hundred of micrometres) were generated when the zinc and sulfur feed rate was 21 g min^{-1} and nitrogen (3 $m^3\ h^{-1}$) was used as the cooling gas. All the synthesized ZnS nanoforms had the hexagonal wurtzite structure. During the synthesis, the residence time of the particles in the plasma, *i.e.*, duration of the reaction, was several seconds; therefore, the growth of nanostructures rapidly ceased.

In the cited experiments,[21] ZnS hollow nanotubes and tetrapods were detected near the reactor wall (Fig. 9); they resulted from partial oxidation of zinc sulfide with atomic oxygen, which was present in nitrogen as an impurity.

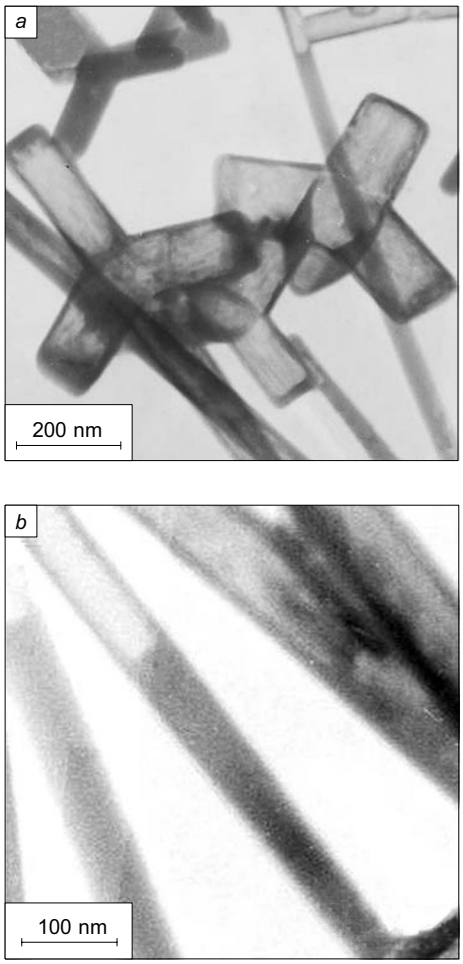


Figure 9. TEM images of ZnS hollow nanostructures: tetrapods (*a*) and nanotubes (*b*).[21]

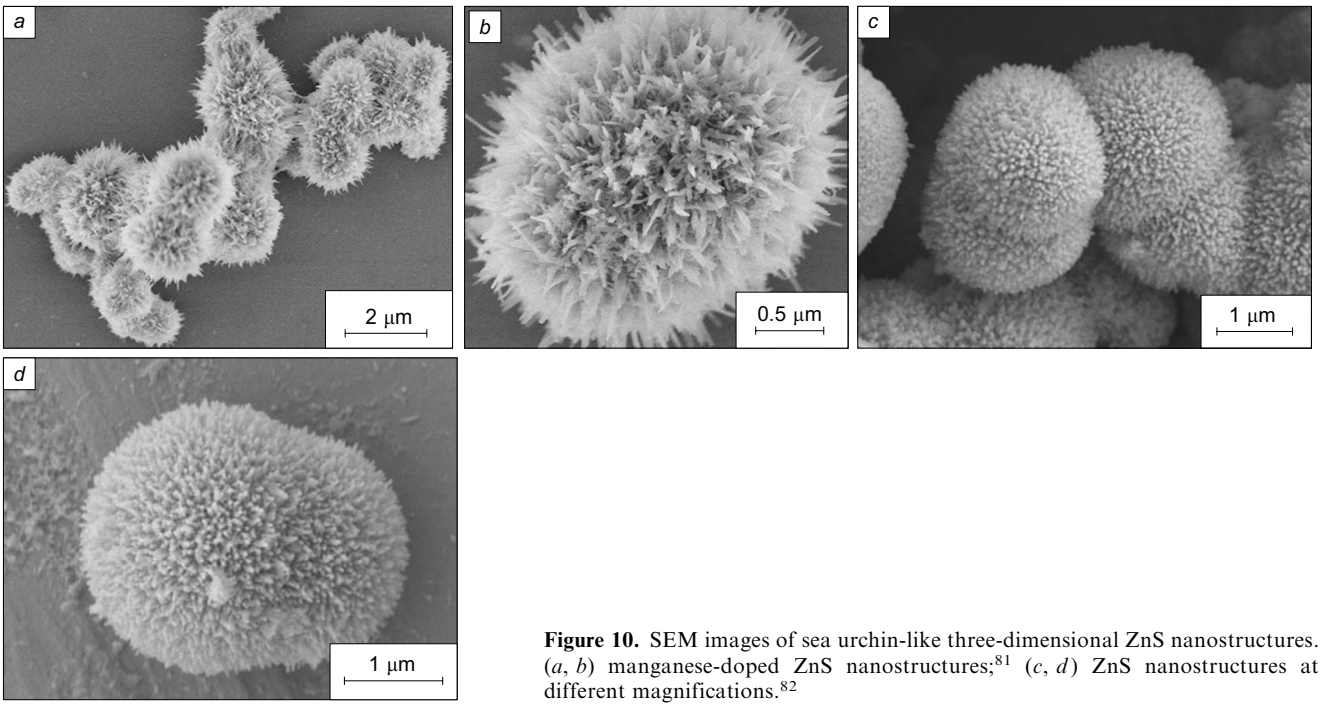


Figure 10. SEM images of sea urchin-like three-dimensional ZnS nanostructures. (*a*, *b*) manganese-doped ZnS nanostructures;[81] (*c*, *d*) ZnS nanostructures at different magnifications.[82]

Three-dimensional ZnS systems composed of one-dimensional nanostructures feature a complex morphology and combine properties of all the involved nano-sized building blocks. The self-assembly of nano-sized blocks into complex three-dimensional nanostructures is the subject of quite a few studies. Among three-dimensional nanostructures, attention is attracted by unique sea urchin-like architectures. A solvothermal process has been proposed

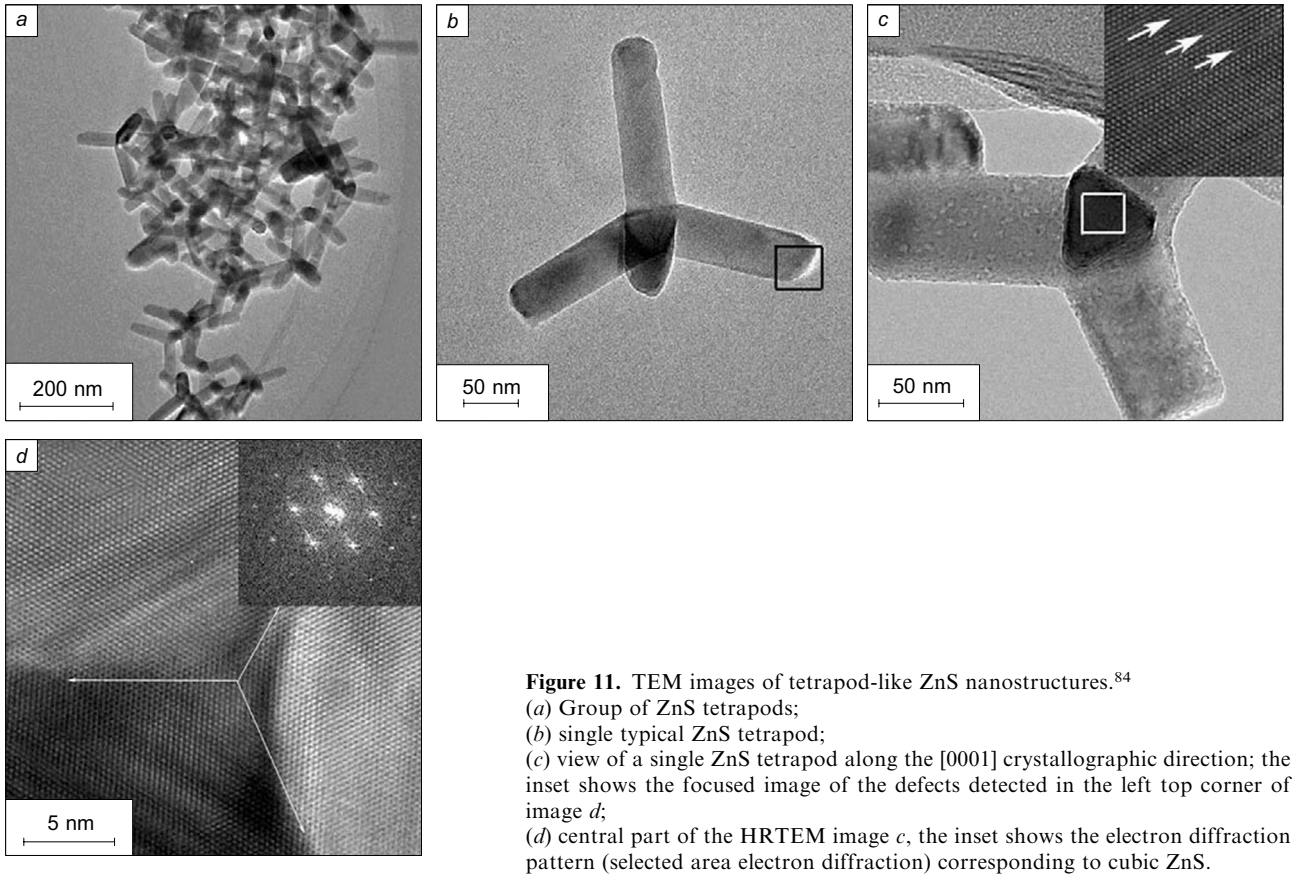


Figure 11. TEM images of tetrapod-like ZnS nanostructures.[84]
(*a*) Group of ZnS tetrapods;
(*b*) single typical ZnS tetrapod;
(*c*) view of a single ZnS tetrapod along the [0001] crystallographic direction; the inset shows the focused image of the defects detected in the left top corner of image *d*;
(*d*) central part of the HRTEM image *c*, the inset shows the electron diffraction pattern (selected area electron diffraction) corresponding to cubic ZnS.

for the fabrication of sea urchin-like manganese-doped ZnS nanostructures [81] (Fig. 10 *a*,*b*). Along with zinc and manganese acetates and thiourea, which served as sources of zinc, manganese and sulfur ions, the reaction mixture contained ethylenediamine and ethanolamine. The synthesis was carried out at a temperature of 430 K for 24 h. The diameter of the resulting sea urchin-like ZnS nanostructures composed of tightly assembled nanorods was 0.5 – 1.5 μm. Xiong *et al.*[82] also prepared three-dimensional ZnS nanostructures resembling the sea urchin body by the solvothermal method at 410 K (Fig. 10 *c*,*d*). The reaction mixture contained zinc acetate, ethanolamine and L-cysteine (as a source of sulfur atoms).

Three-dimensional ZnS nanostructures were reported [16] to exhibit a very high photocatalytic activity: upon IR irradiation, nanostructures are more efficient than ZnS nanopowders, while upon UV irradiation, they are more efficient than TiO_2 nanopowders.

Flower-shaped polycrystalline ZnS nanostructures with a diameter of 800 – 1000 nm have been prepared.[83] Owing to a large specific surface area, these three-dimensional nanostructures are used in gas sensors and for photocatalysis.

Gong *et al.*[84] obtained tetrapodal ZnS nanostructures by the direct reaction of zinc and sulfur vapours at 1370 K in a flow of high-purity nitrogen followed by deposition of the product on a stainless steel mesh at 770 K. The ZnS tetrapods were approximately equal in size and shape (Fig. 11 *a*) and had four branches (legs) of equal length of ~150 nm protruding from the centre (Fig. 11 *b*). The angle between any two legs (~109°) was close to the angle between straight lines drawn from the centre of a regular tetrahedron towards the vertices (109.4°). According to electron microscopy and diffraction data, each leg had a triangular cross-section with a ~30 – 50 nm side. The tetrapod legs had a wurtzite type hexagonal structure, while the central core was a cubic type sphalerite structure, as shown by electron diffraction and by fast Fourier transform of a high resolution transmission electron microscopy (HRTEM) image (Fig. 11 *d*).

Zhai *et al.*[85] prepared ZnS tetrapodal nanostructures by thermal decomposition of $Zn(S_2CNEt_2)_2$ powder at a temperature of 670 K with the subsequent vapour deposition of zinc sulfide and epitaxial growth of ZnS using CdSe nanocrystals as seeds. The resulting tetrapods had a nanocrystalline CdSe core and four ZnS legs with the wurtzite structure protruding from the core along the [0001] crystallographic directions.

Tetrapodal dendrite heteronanostructures of ZnS with an enhanced emission power were also obtained by thermal evaporation of a ZnS powder in an NH_3 atmosphere at 1470 K for two hours.[86]

3.3. Zinc sulfide thin films

Thin films represent a key type of semiconductor optical materials. Sulfide thin films, including ZnS films, are obtained by various methods such as chemical and physical vacuum deposition, successive ionic layer adsorption and reaction,[87 – 89] metal organic chemical vapour deposition,[90] molecular beam epitaxy,[91] aerosol pyrolysis, chemical bath deposition,[92 – 95] pulsed laser deposition,[96] atomic layer epitaxy,[97] magnetron sputtering,[98, 99] ultrasonic spray pyrolysis,[100] sol – gel method, chemical vapour deposition [101] and electrochemical deposition.[102, 103]

It is noteworthy that ZnS films are regarded as buffer layers, alternative to CdS, for the fabrication of polycrystalline $Cu(In,Ga)Se_2$ films of multilayer solar cells.

Doña and Herrero [92] synthesized ZnS films with a cubic structure and high transmittance (> 75%) by deposition from aqueous solutions of zinc sulfate, thiourea and ammonium hydroxide, with hydrazine being used as the complexing agent. Zhou *et al.*[93] deposited a ZnS film on a glass substrate from an aqueous solution also containing $ZnSO_4$, N_2H_4CS and NH_4OH. The resulting films are characterized by a stable transmittance of > 80% in the 600 – 850 nm wavelength range. Hexagonal ZnS thin films were prepared by laser-assisted photochemical vapour deposition using gas-phase decomposition of zinc isopropyl xanthate.[101] The film consisted of small granular particles ~1 μm in diameter formed by nano-sized ZnS grains.

Chemical bath deposition of zinc sulfide films with a cubic structure from aqueous solutions of $ZnSO_4$, N_2H_4CS, NH_4OH and N_2H_4 has been described.[104] For the deposition, the glass substrate was kept for two hours in a reaction mixture heated to 340 K. The grain size of the deposited film was ~5 nm.

Glass-supported thin films of cubic ZnS with a thickness from 100 to ~230 nm were prepared [105] by chemical bath deposition from aqueous solutions of zinc acetate and thioacetamide without any complexing agents at a temperature of ~340 K. The deposition time according to the reaction

$$Zn(OAc)_2 + MeC(S)NH_2 \longrightarrow ZnS\downarrow + MeCN + 2\,AcOH \quad (6)$$

was 120 min. The band gap of the unannealed ZnS film was 3.64 eV; vacuum annealing at a temperature of up to 670 K led to a decrease in E_g to 3.28 eV.

The deposition of ZnS film on a glass substrate from a $ZnCl_2$ and Na_2S in a polyvinyl alcohol matrix has been reported.[106]

The ZnS and ZnS:Mn thin films with a thickness of ~200 nm and a *B*3 type cubic structure were obtained by immersion of a glass substrate into a solution of presynthesized ZnS powder in 2-methoxyethanol (ethylene glycol monomethyl ether) followed by vacuum annealing.[107] A TEM image of an unannealed ZnS film formed by spherical crystallites with an average size of ~3.6 nm is shown in Fig. 12. The band gaps of the unannealed film and

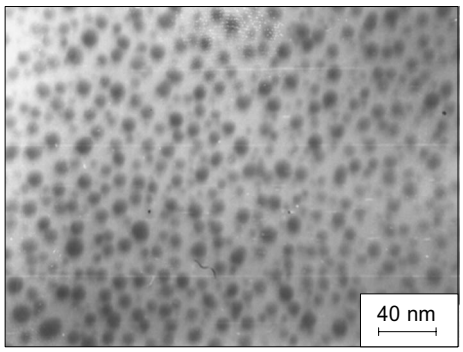


Figure 12. TEM image of unannealed ZnS film with a ~4 nm particle size.[107]

the films annealed at 370, 470 and 570 K were 4.00, 3.87, 3.80 and 3.75 eV, respectively.

The high radiofrequency magnetron sputtering for the growth of high-quality ZnS films utilized for the manufacture of electroluminescent displays allows one to control the film stoichiometry and uniformity. This sputtering technique was used [99] to deposit a ZnS film on a glass substrate. The distance between the target and the substrate was ~ 50 mm; the deposition was carried out in a chamber evacuated down to 6.6×10^{-3} Pa (5×10^{-5} mm Hg). A ZnS target with a diameter of 50 mm was used. For film deposition, the chamber was filled with argon at a pressure of 4 Pa (3×10^{-2} mm Hg); the sputtering power was 120 W. All films grown at different substrate temperatures had a cubic structure and were arranged in the (111) plane. Figure 13 shows a SEM image of a cross-section of a ZnS film deposited on a substrate heated to 370 K. The average size of crystallites varied from ~ 20 to ~ 60 nm as the substrate temperature during deposition changed from 370 to 670 K.

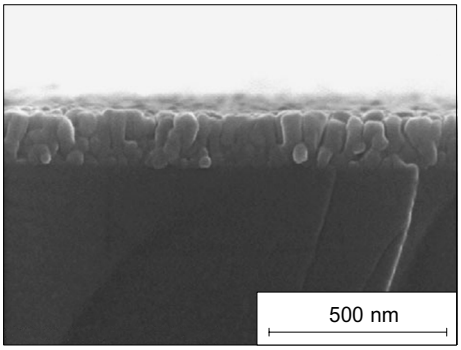


Figure 13. SEM image of the cross-section of a ZnS film magnetron sputtered on a substrate preheated to 370 K.[99]

By doping semiconductor nanostructures and thin films, it is possible to change their physical properties. Zinc sulfide nanostructures are doped by Mn, Cu, Fe, Ni or Co. Kang *et al.*[108] prepared doped ZnS:Mn and ZnS:Fe nanostructures by gas-phase chemical transport using powdered zinc oxide, zinc sulfide and a doping metal chloride. Doped nanowires were deposited on a silicon substrate coated by a gold layer. The deposition of $Zn_{1-x}M_xS$ nanowires follows the scheme presented below

$$ZnO(powder) + MS(powder) + MCl_2 \longrightarrow Zn_{1-x}M_xS\downarrow + Cl_2\uparrow + M_3O_4 \quad (7)$$

where M = Mn or Fe.

3.4. Chemical bath deposition of nanostructured zinc sulfide from aqueous solutions

The nano-sized sulfide materials obtained by chemical synthesis in aqueous media considerably differ from the ZnS-based film materials.[91, 97, 109, 110] The CdS nanocrystals were the first nano-sized sulfides.[46, 111 – 116] The knowledge and experience accumulated in the experimental and theoretical studies of CdS nanocrystals [46, 117 – 122] made it possible to establish their electronic structure and to comprehend and predict the size dependences of their optical properties.

The chemical bath deposition from aqueous solutions, which is also called chemical condensation, one-pot synthesis in aqueous solutions or, more briefly, hydrochemical deposition, is one of the most popular methods for the synthesis of various forms of nanostructured sulfides.[123]

From the chemical standpoint, the aqueous synthesis of semiconductor nanoparticles is as simple as the substrate deposition, except for the fact that control of the initial deposition stage requires a stabilizing agent, which restricts the growth of nano-sized particles. An appropriate stabilizing agent for the synthesis of sulfide nanoparticles can be selected considering any chemical reaction, resulting in the formation of insoluble compounds. This approach can be used to prepare nanoparticles and quantum dots of not only ZnS,[46, 124] but also CdS,[46, 125] PbS [126] or other metal chalcogenides.[127]

In the synthesis of nanostructured zinc sulfide, water-soluble salts, $ZnSO_4$, $Zn(NO_3)_2$, $ZnCl_2$ and $Zn(OAc)_2$, are used as sources of Zn^{2+} ions, while sources of sulfur ions include various soluble sulfides (such as Na_2S) and hydrosulfides, hydrogen sulfide, thiocarbamide (thiourea), sodium thiosulfate, thioacetamide and so on. Solutions of sodium citrate, ethylenediamine, disodium ethylenediaminetetraacetate (Trilon B), which form complex salts with zinc ions, are applied as complexing agents and stabilizers. As a rule, deposition is carried out in an alkaline medium at pH from 9 to 13 – 14, which is adjusted by addition of aqueous ammonia to the reaction mixture.

Most of water-based synthetic routes to nanostructured sulfides involve the use of water-soluble thiols (the sulfur analogues of alcohols with the general formula RSH, where R is a hydrocarbon moiety, *e.g.*, MeSH, EtSH, *etc.*) as the surface ligands.[128] The pH-induced reaction of the thiol with the metal ions of nanoparticles and pH-dependent properties make the aqueous synthesis of semiconductor sulfide nanoparticles more versatile as regards surface functionalization compared with other methods of synthesis.

The key parameters of the aqueous synthesis of semiconductor nanoparticles are as follows:

— ionic product (IP) of the semiconductor compound in water;

— affinity of the metal ions located on the nanoparticle surface for the coating ligands;

— pH of the aqueous medium.

Thiourea is used, most often, for sulfidization during the chemical deposition from aqueous solutions of zinc sulfide and some other sulfides, which is due to its hydrolytic decomposition. In alkaline solutions, thiourea is hydrolyzed to give weak hydrosulfuric acid and cyanamide [129]

$$N_2H_4CS \rightleftharpoons H_2S + H_2CN_2 \quad (8)$$

If metal ions are present in the solution, they form the corresponding sulfides with the S^{2-} ions. For example, $ZnSO_4$, N_2H_4CS and ammonium hydroxide react as follows:

$$ZnSO_4 + N_2H_4CS + 2\,NH_4OH \longrightarrow ZnS\downarrow + H_2CN_2 + (NH_4)_2SO_4 + 2\,H_2O \quad (9)$$

In the presence of complexing agents, intermediate metal complexes can be formed, which then dissociate with

sulfide precipitation. For example, the precipitation of zinc sulfide with thiourea in an alkaline medium in the presence of ethylenediamine as a complexing agent proceeds according to the reaction

$$Zn[C_2H_8N_2]_n^{2+} + N_2H_4CS + 2\,HO^- \longrightarrow \quad (10)$$

$$\longrightarrow ZnS\downarrow + n\,C_2H_8N_2 + H_2CN_2 + 2\,H_2O$$

Spontaneous formation of a metal sulfide is possible if the ionic product

$$IP = [M^{2+}]_0\,[S^{2-}]_0 \quad (11)$$

is higher than the solubility product of this sulfide (K_{sp}); in this case, the solution is supersaturated, with the supersaturation

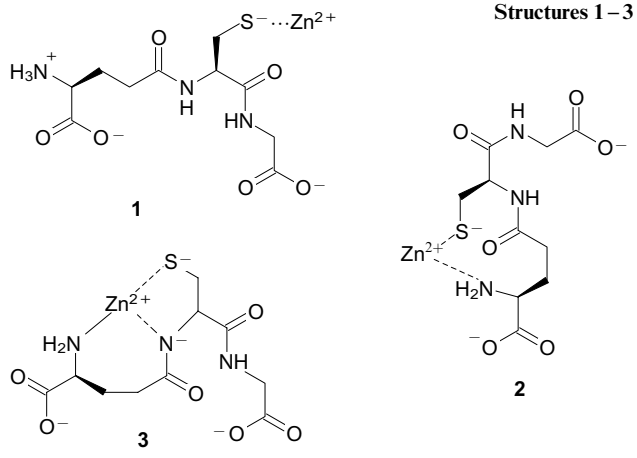
$$S_S = \frac{IP}{K_{sp}} \quad (12)$$

being greater than unity. The solubility product of zinc sulfide ZnS is low: at a temperature of 298 K, $K_{sp} \approx 1.6 \times 10^{-24}$ for α-ZnS and $K_{sp} \approx 2.5 \times 10^{-22}$ for β-ZnS.[130, 131] The low K_{sp} value of zinc sulfide induces its precipitation even from dilute aqueous solutions.

Hedayati *et al.*[132] prepared ZnS nanoparticles by chemical precipitation at a temperature of 350 K from a mixture of aqueous solutions of zinc acetate, thiourea or sodium sulfide, as a source of sulfur, and thioglycolic acid. Additionally, the alkalis NaOH and KOH were used as precipitating agents. The nanoparticle morphology depended on the reactants used. The ZnS nanoparticles precipitated by NaOH or KOH were star-like and had an average size of ~100 and ~200 nm, respectively. The agglomerated ZnS nanoparticles obtained with the use of thioglycolic acid had an average size of ~150 nm. The ZnS nanoparticles synthesized using thiourea were triangular and had an average size of up to 100 nm. Zinc sulfide nanoparticles synthesized with the simultaneous use of thiourea and sodium sulfide also had an average size of up to 100 nm.

The influence of the pH of the aqueous medium on the deposition of nanostructured zinc sulfide and nanoparticle interaction with the complexing agent was demonstrated[133] in relation to the structural evolution of the Zn^{2+} complex with glutathione. The ZnSe/ZnS core/shell nanoparticles were prepared in an aqueous reaction mixture containing glutathione, sodium borohydride, zinc acetate, quinine sulfate dihydrate, L-cysteine, selenium powder and 3-mercaptopropionic acid. When pH is from 6.5 to 8.3, the thiol group SH is the main glutathione coordination site for Zn^{2+} (structure **1**). For the pH range from 8.3 to 10.3, the deprotonated amino group NH_2 additionally promotes the coordination (structure **2**). When pH is from 10.3 to 11.5, the negatively charged nitrogen atom of the CONH group is also involved in Zn^{2+} coordination (structure **3**). The Zn^{2+} coordination to the amide bond nitrogen not only influences the zinc acetate activity as a source of Zn^{2+} ions, but also facilitates the release of sulfur from glutathione, which gives rise to ZnSe/ZnS core/shell nanocrystals.

Structures 1 – 3



3.5. Characteristic features of zinc sulfide formation from solutions and vapours

The principal and evident difference between the syntheses of zinc sulfide nanoparticles from solutions and vapours is the different physical state of the reaction medium. In the former case, the reaction medium is liquid, while in the latter case, nanoparticles are formed in the gas phase (most often, in an inert gas) at a reduced pressure.

The above examples demonstrate that ZnS nanoparticles and nanostructures are prepared using liquid- and gas-phase synthesis techniques. The liquid-phase methods include chemical bath deposition from aqueous or alcohol solutions, sol – gel technique and microemulsion, sonochemical and hydro- and solvothermal syntheses. Chemical bath deposition from solutions is the simplest and the most popular method. Liquid-phase methods are widely used both in laboratory and in industry owing to the possibility of precise control over the reactant composition and concentrations, rather simple equipment and wide diversity and low cost of the obtained products. The chemical bath deposition of ZnS nanoparticles in the presence of stabilizing agents adsorbed on the nanoparticle surface allows the most precise control over the size of isolated nanoparticles and fabrication of a protective shell of organic ligands. The protective shell minimizes the agglomeration, prevents the particle growth and oxidation and increases the size and composition stability of the particles.

The possibility of using stabilizing agents to control the size of the resulting nanoparticles is an important advantage of liquid-phase synthesis in comparison with the gas-phase methods.

The stabilizing agents that ensure the preparation of isolated stable ZnS nanoparticles include TOPO,[47] L-cysteine,[61, 133] 3-mercaptopropionic acid,[133] hexadecylamine,[71] polyethylene glycol,[60] glutathione,[133] sodium citrate and disodium ethylenediaminetetraacetate, which are electrostatic stabilizers and surfactants. The above stabilizing agents are used for the synthesis of both zinc sulfide and isolated nanoparticles of other sulfides — PbS,[5, 6, 123, 127] CdS,[14, 123, 127] Ag_2S[9 – 12, 123, 127] and Cu_2S.[13, 45]

Nanoparticles in colloid solutions are stabilized by introducing agents that modify and coordinate the surface atoms of nanoparticles.[123] For example, when L-cysteine (water-soluble amino acid) is used, the zinc atoms of the sulfide nanoparticle are complexed with cysteine coating the ZnS surface *via* amino groups.[61]

Nanoparticles in nonaqueous solutions are often stabilized by TOPO.[47] However, these stabilized nanoparticles are soluble only in organic solvents; hence, for applications in biological media, *i.e.*, for endowing the nanoparticles

with water solubility, hydrophilic groups are additionally attached to their surface. For example, the hydrophobic TOPO molecules located on the nanoparticle surface bind to the hydrophobic parts of polyethylene glycol, while the hydrophilic PEG groups, which point to the surrounding aqueous solution, form the isolating polar shell. Polyethylene glycol was used as the stabilizer in the hydrothermal synthesis of ZnS microspheres.[69]

3-Mercaptopropionic acid and glutathione were employed together[133] as stabilizing agents for the deposition of isolated ZnSe/ZnS core/shell nanoparticles of ~5 nm size from aqueous solutions. Stabilization was accomplished by SH and NH_2 coordination to the zinc atoms.

The manganese-doped water-soluble ZnS : Mn quantum dots were synthesized[134] using 3-mercaptopropionic acid as the stabilizing agent.

The key features of the preparation of nanoparticles by evaporation and condensation are as follows:

— nanoparticle formation upon cooling of the vapour in the condensation zone;

— considerable effect of convective gas flows on the condensation;

— fast increase in the average nanoparticle size with increasing gas pressure.

Chemical vapour deposition is accomplished *via* high-temperature decomposition reactions and/or reactions of gaseous reagents in the reactor or on a substrate. The deposition of ZnS nanoparticles from the gas phase is performed using starting compounds characterized by high vapour pressure at relatively low temperatures and compounds that readily decompose at elevated temperature such as organometallic compounds, *e.g.*, $Zn(S_2CNEt_2)_2$.[67] For the physical deposition of nanostructured ZnS from the gas phase, in particular, by thermal evaporation, zinc sulfide powder is often used.[66, 75 – 79]

The vapour deposition of ZnS nanoparticles features high productivity and is able to produce nanostructures (including nanofilms for luminophores) with a Zn : S ratio varying from ~0.95 to ~1.20.[99] Meanwhile, vapour deposition, unlike bath deposition, requires more complicated equipment and higher temperatures, which leads to higher cost of the final products. Due to metastability of gas-phase deposition processes, it is difficult to control the size and shape of nanostructures.

4. Control of morphology of zinc sulfide nanostructures

The morphology of ZnS nanostructures appreciably depends on the preparation method and their composition and crystal structure. In the general case, the particle morphology is dictated by their growth kinetics and minimization of their surface energy. As a rule, nanoparticles are thermodynamically non-equilibrium,[45] their diverse morphology being a consequence of metastability, *i.e.*, occurrence of the system in one or another local minimum of free energy.

According to Akiyama *et al.*,[135] in the case of the smallest ZnS nanoparticles, the particle size predetermines the crystal structure: for < 4 nm ZnS nanoparticles, the hexagonal wurtzite (*B*4 type) structure is more stable than the cubic sphalerite structure. The change in the morphology with increasing particle size from nano- to micrometre range has been analyzed.[136]

The shape of nanocrystalline particles can be controlled by varying the kinetic parameters of the synthesis such as temperature, pressure, reactant concentration, synthesis duration, solution supersaturation and pH, heating and cooling rates and the presence of surfactants or other additives.

The primary cause of anisotropic shape of the nanoparticles being formed is anisotropy of the liquid or gaseous medium in which different reactant fluxes are supplied to different faces of the growing nucleus. For example, nanocrystals that precipitate from solutions on the bottom of a vessel acquire an anisotropic shape, whereas the nanoparticles that are suspended in the reaction solution are normally spherical. During the deposition of nanocrystals from the gas phase onto a substrate, the surface diffusion of reactant gas fluxes is usually anisotropic; this results in the formation of nanocrystals with anisotropic morphology (nanorods, nanoribbons, nanotubes, star-like nanoparticles and so on). Other sources of anisotropic morphology can also exist (*e.g.*, the presence of defects, coalescence). Indeed, the presence of screw dislocations increases the nanocrystal growth rate in one direction. The presence of dislocations in two mutually perpendicular directions induces growth of plate nanoparticles. The shape of the resulting nanoparticles is also affected by impurities.[137, 138]

A key mechanism of control over the crystal morphology is the targeted action on the growth of particular faces.

According to Tong *et al.*,[61] a higher growth rate along the normal direction is inherent in crystal planes with a higher surface energy. Although this statement is supported by some experimental and theoretical data, it cannot be taken as being completely true. According to molecular dynamics data for the surface energies of ZnS crystals,[139] the predominant direction of the kinetic growth for hexagonal ZnS crystals is [001], *i.e.*, they mainly grow along the *c* axis.

For example, according to experiments,[80] ZnS nanobelts with the wurtzite structure, prepared by solvothermal deposition on a zinc substrate, grew in the [0001] direction (that is, along the hexagonal *c* axis), namely, at right angle to the substrate, which also had a hexagonal structure. The authors noted that zinc foil used as the substrate ensured the predominant growth of nanobelts along the [0001] direction.

The arrays of hexagonal ZnS nanobelts were grown[79] by thermal evaporation of a pressed zinc sulfide nanopowder, which served as not only the source of ZnS clusters, which evaporate at high temperature, but also as the substrate with numerous nucleation sites. Owing to the hexagonal structure of the substrate, the epitaxial growth of ZnS nanobelts occurred along the [001] direction.

The growth of uniform ZnS nanorods was accomplished[21] with identical feeding rates of the zinc and sulfur powders to be evaporated. The resulting < 4 nm ZnS nuclei had a hexagonal structure, which is consistent with other reported data.[135] These nuclei grew to form hexagonal nanorods.

Sphalerite type ZnS nanowires were grown[65] using thermal evaporation of zinc and sulfur and subsequent autocatalytic homoepitaxial growth of a one-dimensional cubic ZnS structure along the [111] direction. In other

words, the predominant growth of cubic ZnS nanowires occurred in the planes with the highest reticular density.

The nanoparticle growth and morphology are markedly affected by the process conditions. The effect of heating rate of the reaction mixture on the crystal structure and morphology of the resulting ZnS nanoparticles has been studied.[140] The nanoparticles were prepared using a mixture of solutions of ZnI_2 in oleylamine and sulfur in octadec-1-ene. The reaction mixtures were heated to 470 K at different rates and kept at this temperature for an hour. When heating was slow (0.01 K s^{-1}) and the temperature was ~400 K, hexagonal ZnS nanorods were formed in the reaction mixture; during the subsequent heating to 470 K, they reached the length of ~10 nm and a diameter of ~4 nm and gradually acquired a cubic structure. When heating was fast (500 K s^{-1}), cubic ZnS nanoparticles 3 – 4 nm in diameter were directly formed in the reaction mixture. The variation of the heating temperature, especially in the initial stage, determined both the crystal structure and the morphology of resulting ZnS nanoparticles.

A publication of Wang *et al.*[141] addresses the effect of surfactant concentration on the morphology of ZnS nanoparticles obtained by the solvothermal method. Zinc sulfide was synthesized in an autoclave at 430 K for 12 h from a mixture of zinc acetate and thiourea solutions in water or ethylenediamine with addition of the $C_{12}H_{25}SO_3Na$ surfactant. In the absence of the surfactant, ZnS particles with plate morphology were formed; when the surfactant concentration was 0.035 mol $litre^{-1}$, flow-shaped ZnS microspheres were obtained, while for the surfactant concentration of 0.105 mol $litre^{-1}$, large microcrystals were generated.

The effect of solvents (ethanolamine and ethylenediamine) on the morphology of ZnS micro- and nanospheres precipitated from solutions at 470 K was studied in detail.[61] Microspheres obtained from solutions with different concentrations of ethanolamine and ethylenediamine were composed of ZnS blocks with different crystal structures and shapes. For example, at the ethylenediamine : water volume ratio of 1 : 50, cubic nanospheres were assembled from ZnS quantum dots, while the 1 : 10 ratio resulted in nanospheres assembled from a mixture of quantum dots, nanosheets and nanorods with cubic and hexagonal structures. The replacement of ethylenediamine by ethanolamine with an ethanolamine : water volume ratio of 1 : 50 resulted in nanospheres composed of hexagonal ZnS nanorods, while the ethanolamine : water ratio of 1 : 10 gave rise to single hexagonal ZnS nanorods. Thus, increasing the concentration of ethylenediamine or ethanolamine was accompanied by the predominant formation of hexagonal nanorods growing along the [001] direction.

In the bath deposition of ZnS nanostructures, the nanoparticle morphology is affected by the pH value. The ZnS nanoparticles produced by hydrothermal precipitation from aqueous solutions of zinc acetate, thiourea and thioglycolic acid[132] were roundish agglomerates of 150 – 200 nm size. Increasing the solution pH by adding NaOH afforded star-like ZnS particles of ~100 nm size.

The key processes used to prepare ZnS nanostructures with different morphology are characterized in Table 2.

The performed analysis shows that several qualitative trends can be distinguished in the control of the morphology of ZnS nanostructures; however, this problem has not been generally solved as yet. This is true for nanostructures of not only zinc sulfide, but also other sulfides with diverse morphology, *e.g.*, lead sulfide.[6, 123, 127, 142, 143]

Table 2. Methods for the synthesis of ZnS nanostructures with different morphology.

Main reactants	ZnS nanostructure morphology	Scope of application	Advantages of the method	Disadvantages of the method	Ref.
		Solvothermal synthesis			
$ZnCl_2$, S, $C_{18}H_{37}N$, $C_{24}H_{51}OP$, N_2H_4CS, $C_2H_6O_2$	Nanocrystals (quantum dots)	Optical devices	Manifestation of the quantum size effect	Low product yield	47, 48
		Hydrothertmal synthesis			
$ZnSO_4$, Na_2S	Nanopowder of spherical particles	Biological sensors	Blue shift in the UV spectrum	High temperature of the synthesis	49
$Zn(OAc)_2$, N_2H_4CS	Hollow nanospheres	Biological sensors	Template-free synthesis	Large diameter of the nanospheres (up to 300 nm)	57
		Hydro- and solvothermal syntheses			
$Zn(NO_3)_2$, L-cysteine, C_2H_7NO, $C_2H_8N_2$	Nanospheres assembled from cubic and hexagonal nanorods	Optical devices	Simplicity of the synthesis	Large size and broad size distribution of the nanostructures	61
		Hydrothertmal synthesis and ageing in the reaction mixture			
$ZnEt_2$, S, hexadecylamine	Nanospheres and nanorods	Optical devices	Manifestation of the exciton size effect	Broad size distribution of the nanostructures	69

Table 2 (continued).

Main reactants	ZnS nanostructure morphology	Scope of application	Advantages of the method	Disadvantages of the method	Ref.
			Thermal evaporation		
ZnS powder, gold film	Nanowires and nanorods	UV sensors	Narrow size distribution of the nanostructures	High temperature of the synthesis, high cost of the product	66
Pressed ZnS powder, Ar	Nanobelts and orientation-ordered nanobelt arrays	Field emitters	Template-free synthesis, high emission current density (14.6 mA cm^{-2})	High temperature of the synthesis	79
Zn foil, S powder, Ar	Nanowire array	Field emitters	High enhancement factor (1530)	High temperature of the synthesis	65
ZnS powder	Dendrite-like tetrapods	Field emitters	Low turn-on voltage, high enhancement factor (2600)	High temperature of the synthesis, ammonia atmosphere	86
			Chemical vapour deposition with thermal decomposition of the precursor		
$Zn(S_2CNEt_2)_2$, Au nanoclusters	Nanowires	UV sensors	High product yield	High product cost	67
			Thermal evaporation, chemical vapour deposition		
ZnS, Ar, H_2, C	Nanobelts	UV sensors	High spectral sensitivity	High temperature of the synthesis	75 – 77
			Chemical vapour deposition		
ZnS, C, S powders	Nanobelts	Field emitters	Ultrathin nanobelts with high aspect ratio	Low product yield	78
			Solvothermal synthesis followed by heat treatment		
$Zn(OAc)_2$, N_2H_4CS, $C_2H_8N_2$, Zn foil	Nanobelt array	Field emitters	Narrow length and thickness distributions, high aspect ratio	Low emission current density	80
			Chemical bath deposition from aqueous solutions		
$ZnSO_4$, N_2H_4CS, NH_4OH	Film	Optoelectronics	> 80% transmittance in the IR range	ZnO contamination	93
			Magnetron sputtering		
ZnS, Ar	Film	Buffer layer for solar cells	> 80% transmittance in the visible range	Sophisticated equipment	99

5. Properties and application of nanostructured zinc sulfide

Photo- and electroluminescence are important properties of zinc sulfide; ZnS is considered to be one of the best fluorescent semiconductor materials for luminescent devices. Luminescence is light emission not associated with heating, but caused by conversion of the energy absorbed by a substance into optical emission energy. Depending on the excitation mechanism, luminescence is classified into several types, among which electro- and photoluminescence are most common in semiconductor photonics. Photoluminescence is excited by visible light with different wavelengths, electroluminescence is excited as electricity is passed through the material (this is one of the few examples where electrical energy is directly converted into visible light without heating or chemical reaction).

The electroluminescent properties of zinc sulfide were initially studied using single crystals and coarse-crystalline powders.[144 – 146] The electroluminescence of ZnS noticeably depends on temperature and magnetic field strength. The electroluminescence intensity increases with increasing temperature. This is due to the temperature dependence of the generation of primary electrons needed to excite the luminescence [145] under the action of a magnetic field.[147]

The results of studies of electroluminescent properties of coarse-crystalline ZnS suggest that ZnS-based semiconductor nanocrystals would be promising luminophores for new-generation electroluminescent devices. In particular, considerable advances were made in the design of thin-film nanocrystalline semiconductor light emitting diodes (LEDs). Thin-film electroluminescent devices consist of a luminophore layer (manganese-doped zinc sulfide ZnS : Mn) and a Si_3N_4 insulating layer, which are located between an aluminium metal electrode and a transparent ZnO : Al electrode supported on a glass substrate (Fig. 14).

The Si_3N_4 and ZnO : Al layers of 30 and 130 nm thickness were deposited on the glass substrate by magnetron

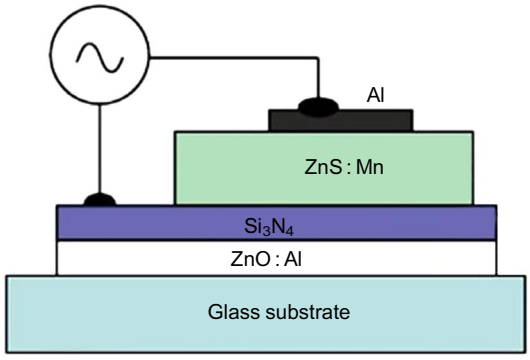


Figure 14. Diagram of an electroluminescent device with a printed emission layer of ZnS : Mn nanoparticles dispersed in an organic solvent.[148]

sputtering. Toyama *et al.*[148] fabricated the nanocrystalline ZnS : Mn luminophore by coprecipitation from a mixture of solutions containing Zn^{2+}, S^{2-} and Mn^{2+} ions and the lauryl phosphate n-$C_{12}H_{25}PO_4H_2$ as the coating agent. For the preparation of printing ink, powdered ZnS : Mn nanoparticles were dispersed in a mixture of a resin and an organic solvent. A layer of this ink supported on Si_3N_4 was dried at a temperature of 400 K.

On application of a rather high voltage, the electrons captured at the interface between the conducting layers migrated to the luminophore and excited the luminescence centres. In the electroluminescence spectrum of the ZnS : Mn nanostructure, the luminescence peak was observed at ~595 nm, while the characteristic electroluminescence defined as the luminescence at a threshold voltage of 45 V decreased with increasing nanoparticle size.[148] The passivation of the ZnS nanocrystal surface enhanced the luminescence.[149]

The practical use of electroluminescent devices based on nanostructured ZnS requires an increase in the luminescence efficiency, which is still lower than that of organic LEDs. The potential benefits of devices based on nanostructured ZnS are high stability and strength and spectrally pure emission colour.

An important trend of semiconductor photonics is development of biocompatible photoluminescent nanomaterials, which would expand the scope of traditional optical methods of biomedical visualization based on the use of organic dyes and fluorescent proteins as markers of biological structures and processes in cells and tissues. Fluorescence dye labelling is a specific application of probing in biological systems. The use of fluorescent nanomaterials based on ZnS and ZnO may improve the location of examined tissues.

The exciton binding energy in zinc sulfide is 39 meV,[150] which is higher than the thermal energy $kT = 26$ meV at room temperature. Therefore, exciton emission can arise at low excitation energy. According to literature data, photoluminescence spectra of many one-dimensional ZnS nanostructures with different morphology show two (or more) characteristic emission peaks. For example, the photoluminescence spectra of single-crystalline ZnS nanoparticles were reported[151] to exhibit a stable intense green emission band at ~513 nm and a weak blue emission band at ~447 nm. In the photoluminescence spectra of hexagonal ZnS nanobelts with a 40 – 120 nm width, 20 nm thickness and a length of several micrometres, two emission bands (around 450 and 600 nm) were detected.[152] In the authors' opinion,[152] the ~450 nm band is associated with ZnS defects, while the ~600 nm band is due to the impurity states of the Mn^{2+} ions. Zinc sulfide nanostructures such as nanorods, nanowires, nanobelts and nanosheets were fabricated by evaporation of ZnS nanopowders in an argon atmosphere at 1370 K. The photoluminescence spectra of the ZnS nanorods and nanowires are identical and show an intense green emission band at 530 nm and a weak blue emission band at 440 nm (Fig. 15 *a*). The ZnS nanobelts and nanosheets also exhibit spectra with almost identical positions of bands, 545 and 440 nm. According to Li *et al.*,[154] the spectrum of ZnS nanosheets contains an intense

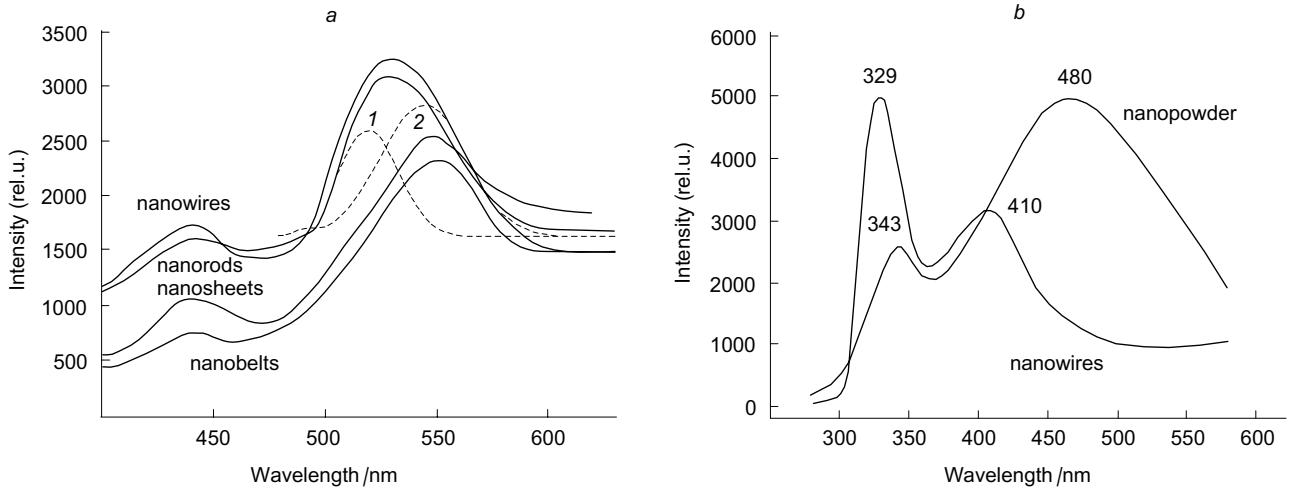


Figure 15. Photoluminescence of ZnS nanostructures.
(*a*) In the visible region, *1* and *2* the photoluminescence spectrum of ZnS nanorods fitted by two Gaussians;[153] (*b*) in the UV and visible regions.[158]

emission band at 534 nm, while the spectrum of ZnS nanorods shows two emission bands at 520 and 578 nm.

The photoluminescences spectrum of 50 – 150 nm CdSe/ZnS microspheres showed an emission band at 625 nm.[155] Generally, the photoluminescence spectrum of water-soluble CdSe/ZnS microspheres resembles the spectrum of hydrophobic CdSe/ZnS quantum dots in an organic solvent.

Considering the photoluminescence duration and high quantum yield, the manganese-doped semiconductor nanocrystals are potential emission sources for the application in optoelectronic devices and biosensors. Zheng *et al.*[156] investigated the effect of temperature and duration of annealing on the photoluminescence of MnS/ZnS core/shell nanoparticles. An increase in the annealing temperature from 490 to 570 K and annealing duration from 40 to 80 min led to decreasing photoluminescence intensity as a result of diffusion of Mn^{2+} ions from the MnS core to the shell surface. In view of this fact, the authors assumed that high-performance MnS/ZnS luminescent nanostructures are to be prepared by short-term annealing at a temperature not exceeding 470 K.

The photoluminescence of nanostructured zinc sulfide was observed not only in the visible, but also in the UV region. The intense UV doublet at 329 – 375 nm (corresponding to the 3.68 – 3.75 eV energy) and a finer structure in the 410 – 480 nm range (corresponding to the 2.44 – 3.06 eV energy) were noted in the luminescence spectrum of ZnS nanowires several tens micrometres long, with a ~55 nm wide rectangular cross-section and a hexagonal structure.[157] An intense UV photoluminescence peak was detected at 329 nm[158] in a study of ZnS nanowires with periodically alternating twins (Fig. 15 *b*).

The luminescence of nanoparticles can be controlled by varying their size and morphology; therefore, quantum dots and other ZnS semiconductor nanostructures are used to develop humidity sensors, gas and chemical sensors and biosensors.

The applicability of ZnS nanowires for measuring the relative air humidity at room temperature has been demonstrated.[159] The increase in the relative humidity from ~30% to ~55% led to some decrease in the nanowire resistance, while further humidity increase to 100% induced a decrease in the resistance by a factor of almost 1000 (Fig. 16 *a*). High sensitivity of porous ZnS nanowires to humidity is caused by their large surface area, which adsorbs moisture from air. The measurement of the relative air humidity by means of aluminium-doped zinc sulfide nanowires ZnS : Al has been investigated.[160] The measurements were carried out at room temperature and relative humidity varying from 30% to 90%. The increase in the humidity in the range from 50% to 90% was accompanied by a nearly proportional decrease in the nanowire resistance caused by physical adsorption of moisture.

A minor oxygen impurity in the inert gas induces surface degradation of the semiconductor in the inert gas atmosphere as a result of oxidation; therefore, accurate *in situ* measurements of an oxygen concentration in the inert gas are required. Liu *et al.*[161] determined the content of oxygen using ZnS nanobelts obtained by evaporation of zinc sulfide. The measurements carried out at an oxygen pressure from 3×10^{-3} to 10^5 Pa and on exposure to UV radiation demonstrated that the conductance of ZnS nanobelts is proportional to the logarithm of oxygen pressure.

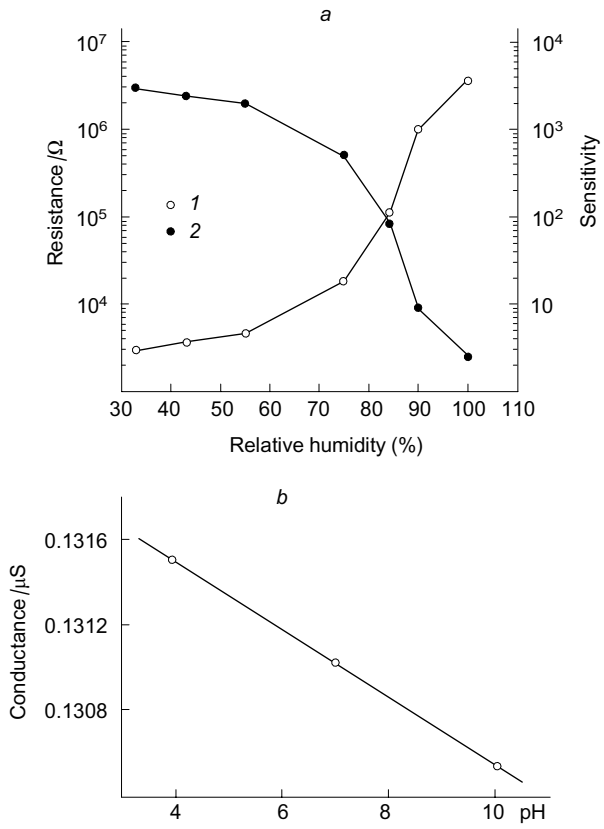


Figure 16. Change in the resistance and sensitivity of ZnS : Al nanowires *vs.* relative air humidity (*a*)[159] and conductance of ZnS/SiO_2 nanocables *vs.* pH of the solution (*b*).[164]

Sensors for the detection of hydrogen and tetrachloromethane impurities based on nanostructured ZnS have been reported.[162, 163]

Due to the small size of semiconductor nanoparticles, their optical properties can markedly change in the presence of only several molecules of a particular compound. Hence, semiconductor nanostructures can serve as chemical sensors.

The nanocables consisting of zinc sulfide nanowires coated by an insulating silica layer and chemically modified by amines feature a linear dependence of conductance on the solution pH. These nanostructures can serve as chemical sensors.[164] They have reproducible electronic characteristics, while the SiO_2 shell protects ZnS nanowires from oxidation. The measurements of the conductance of the ZnS/SiO_2 nanocables performed for buffer solutions with different pH demonstrated a linear pH dependence of the conductance in the pH range from 4 to 10 (Fig. 16 *b*).

The L-cysteine-coated ZnS quantum dots were used as fluorescent sensors for Cu^{2+} ions.[165] The optimal fluorescence intensity was attained at pH 5 and at a nanoparticle concentration of 2.5 mg litre^{-1}. The limit of detection of Cu^{2+} ions by cysteine-coated ZnS quantum dots was higher than that of CdSe/CdS quantum dots with the same cysteine coating.

Devices based on CdSe/ZnS quantum dots are used as fluorescent sensors for phenols in water[166] and for Pb^{2+} ions. It was shown[167] that the replacement of Zn^{2+} ions in the quantum dot shell by Pb^{2+} induces quenching of

quantum dot fluorescence, with fluorescence intensity being linearly dependent on the Pb^{2+} concentration in the range from 0.03 to 3.30 μmol litre^{-1}.

The manganese-doped zinc sulfide nanocrystals coated by an amine layer were used [168] for the fluorescent detection of traces of 2,4,6-trinitrotoluene (TNT) *via* quenching of the intense orange photoluminescence of Mn^{2+} ions. The amine-coated nanocrystals can bind TNT species located in solution or in air *via* interaction of the amine ligands with the TNT aromatic rings. The TNT anions thus generated, which are linked to the amine monolayer, quench photoluminescence of Mn^{2+} ions as a result of electron transfer from the ZnS conduction band to the lower unoccupied molecular orbital of TNT anions. The amine-coated nanocrystals are able to detect down to 1 nmol litre^{-1} of TNT in solution or several parts per billion of TNT in atmospheric air. The chemical sensors based on ZnS : Mn are stable in solutions and in air, show high quantum yield and are effective for detection of traces of TNT and other aromatic nitro compounds.

Biosensors as devices for detection of molecules of particular substances comprise a biological component and a physicochemical detector. The key requirements to a biosensor include identification of the target molecule and the presence of a biological recognition site. He *et al.*[164] synthesized the ZnS/SiO_2 nanocables and employed them to quantify some biological products. The measurements showed that the conductance of biotin-modified nanocables in a phosphate buffer does not vary with time, but rapidly drops almost tenfold as serum albumin is added to the buffer. The authors [164] demonstrated the ability of ZnS-based nano-sized biosensors to detect minor amounts of proteins.

The CdSe/ZnS core/shell quantum dots can be synthesized and conjugated with enzymes, for example, with glucose oxidase.[169] The conjugated CdSe/ZnS quantum dots were used as probes for glucose determination, as increasing the glucose concentration quenched the fluorescence of quantum dots. The quenching is based on electron transfer from the quantum dots to enzyme molecules, which catalyze glycose oxidation and reduction reactions. The CdSe/ZnS quantum dots can replace fluorescent dyes such as ruthenium complexes, which are used in the conventional methods of glucose determination.

Medical diagnosis of kidney and liver diseases requires determination of urea content in blood serum. For this purpose, Huang *et al.*[170] proposed using CdSe/ZnS quantum dots stabilized with mercaptosuccinic acid mixed with urease, a natural enzyme that hydrolyzes urea to give ammonium carbonate. The detection was based on enhancement of the photoluminescence of quantum dots correlated with the enzymatic degradation of urea.

Manganese-doped water-soluble ZnS : Mn quantum dots of ~200 nm size stabilized by 3-mercaptopropionic acid mixed with a bacterial enzyme, arginine deiminase, were proposed for detection of arginine in fruits and fruit juices.[171] Arginine is one of the key amino acids present in most simple proteins. It was ascertained that the fluorescence intensity of quantum dots linearly increases with increasing concentration of arginine in a buffer solution in the range from 10^{-4} to 1.0 mol litre^{-1}.

Tarish *et al.*[172] proposed high-performance sensors for glucose based on ordered heterogeneous arrays of core/shell ZnO/ZnS nanotubes. They found that electrodes modified with zinc sulfide possess an excellent electrochemical response to ferrocyanide/ferricyanide ions and to glucose. The fabricated glucose biosensor showed good results in the glucose concentration range from 2.39×10^{-5} to 2.66×10^{-4} mmol litre^{-1}. The biosensor sensitivity [~188 μA cm^{-2} (mmol litre^{-1})$^{-1}$] exceeded that of the biosensor based on a ZnO nanotube array. The lower limit of detection of glucose, 24 μmol litre^{-1}, was approximately the same as that of a standard electrode. Hence, the fabrication of a nanostructured ZnS shell can increase the compatibility of the ZnO surface with a biological medium.

Thus, the operation of most humidity sensors, gas and chemical sensors and biosensors involving ZnS nanostructures is based on the recording of some signal (emission intensity, resistance, conductance, *etc.*) and the change of the signal in the presence of the analyte (compound, molecule, ion or moisture). The changes in resistance (conductance) of ZnS nanostructures are utilized to determine minor amounts of oxygen, air humidity and pH of the medium (see Fig. 16);[159–163] the optical detection of compounds is based on changes in the fluorescence intensity.[165–171]

Zhao *et al.*[173] fabricated electrodes on the basis of nanostructured ZnS microspheres and sea urchin-like architectures for electrochemical and photoelectrochemical determination of uric acid in aqueous solutions. The electrochemical biosensor based on ZnS sea urchin-like nanostructures showed the highest sensitivity of ~76 μA cm^{-2} (mmol litre^{-1})$^{-1}$. The broad range of determination of uric acid from 0.01 to 1.7 mmol·litre^{-1} corresponds to the requirements of clinical diagnosis. On exposure to radiation at 300 nm, the sensitivity of uric acid determination by this biosensor increased fivefold and reached ~414 μA cm^{-2} (mmol litre^{-1})$^{-1}$, which exceeded the sensitivity of most of modern electrochemical biosensors.

Zinc sulfide nanoparticles are highly chemically stable to oxidation and hydrolysis; therefore, they are of interest as catalysts for decomposition of organic water pollutants, particularly, dyes (rhodamine, methylene blue), ethanol and halo-substituted benzenes.[174] Studies showed that ZnS nanostructures are good photocatalysts; they are capable of fast generation of electron–hole pairs and have negative reduction potentials for excited electrons. Hu *et al.*[174] studied the photocatalytic activity of common and nanoporous ZnS nanoparticles. The nanoparticles with a diameter of ~60 nm had a nearly spherical shape and rather large specific surface area (~156 m^2 g^{-1}); they consisted of aggregates of 3–5 nm nanoparticles with hexagonal structure, with the pore size being < 5 nm. Comparative studies of the catalytic decomposition of eosin demonstrated that nanoporous particles were more catalytically active than usual ZnS nanoparticles.

Zinc sulfide nanoparticles featuring photocatalytic activity towards ethanol decomposition can be used in fuel cells. The enthalpy of ethanol oxidation is several times higher than the zinc sulfide oxidation enthalpy; therefore, in the presence of ethanol, ZnS is not oxidized and can function as a stable catalyst for ethanol oxidation.[175] It is known that ethanol is formed upon fermentation of many organic compounds; therefore, according to Bredol and Kaczmarek,[176] the use of nanostructured ZnS as an electrocatalyst of ethanol oxidation is quite promising.

Light emitting diodes — solid-state lighting devices — attract attention due to low power consumption, high performance and long service life. Among various luminophores, semiconductor quantum dots are most promising as emitters for displays and solid-state lighting devices.[177 – 179] High-performance LEDs with intense green emission were developed [179] on the basis of CdSe/ZnS quantum dots. Green LEDs with different electroluminescence wavelengths (515, 528 and 550 nm) were fabricated using quantum dots that somewhat differed in the composition (cadmium selenide to zinc sulfide ratio). The bright green emission of the LED is due to the unique structure of the CdSe/ZnS quantum dots with a uniform high coverage of the core.

Jang *et al.*[180] fabricated the CdSe/ZnS/CdSZnS and CdSe/CdS/ZnS/CdSZnS nanostructures, which emitted green and red light, respectively.

Zinc sulfide nanostructures are considered to be promising for the design of various solar cells such as dye- or quantum dot-sensitized Cu(In,Ga)Se_2-based thin-film solar cells and hybrid organic-inorganic solar cells.

In the last two decades, wide band-gap semiconductors, TiO_2, CdS and ZnO, have been used as anode materials for dye- or quantum dot-sensitized solar cells. Nanostructured ZnS can also be employed in solar cells as a photoanode. Indeed, CdSe nanocrystals coated by a zinc sulfide shell exhibit intense photoluminescence, which allows the use of CdSe/ZnS nanostructures in solar cells.[181] The efficiency of dye-sensitized solar cells was increased by using nanostructures composed of ZnS-coated ZnO nanowires.[182, 183] The efficiency of a solar cell increases because the ZnS layer that coats the ZnO nanowires suppresses the recombination of injected electrons at the interface between zinc sulfide and zinc oxide.

Solar cells sensitized by quantum dots are most promising. In particular, the use of multilayer (or composite) sensitizers based on nanostructured CdSe or CdS with a ZnS passivation layer enhanced the performance of solar cells.[184]

Among thin-film solar cells with high efficiency, mention should be made of the Cu(In,Ga)Se_2-based cell. This is a multilayer solar cell comprising metal (*e.g.*, molybdenum and aluminium) layers, which serve as electrodes and are separated by an absorbing active semiconductor and buffer layers. The buffer layer is usually made of cadmium sulfide. However, cadmium is toxic; therefore, it was proposed to replace CdS by zinc sulfide. A diagram of a thin-film multilayer solar cell based on Cu(In,Ga)Se_2 with the ZnS buffer layer is depicted in Fig. 17.

The ZnS buffer layer retards the back transfer (or recombination) of electrons between the active layer and ZnO. The ZnS buffer layer can be fabricated by various deposition procedures. When a nanostructured ZnS buffer layer is used in thin-film solar cells, the efficiency of solar energy conversion to electricity may reach ~18%.[175] The increase in the solar cell efficiency is caused by appearance of Zn^{2+} in the buffer layer.

The above results demonstrate that various types of nanostructured zinc sulfide are used in devices for different purposes. For optoelectronic devices, one-dimensional nanostructures are most popular.[185, 186] For example, arrays of one-dimensional ZnS nanostructures (nanobelts, nanowires, nanocables, *etc.*) are used as parts of field emitters and field effect transistors.[78 – 80, 137, 158] Nanostructured films are applied in solar cells.[99, 107, 181, 182] In gas and chemical sensors and biosensors, quantum dot and spherical nanoparticle arrays are used most commonly.[168 – 171, 187] Thus, the morphology of nanostructures is among the factors determining their potential applications.

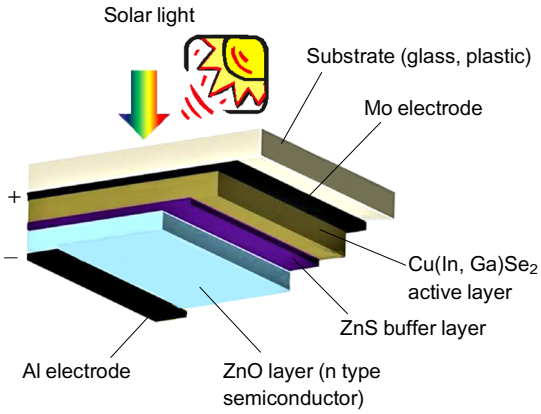


Figure 17. Schematic diagram of a thin-film solar cell based on Cu(In,Ga)Se_2 with a ZnS buffer layer. The Figure was composed by the author using the data of Ref. 17.

6. Conclusion

Zinc sulfide is a versatile semiconductor material [188 – 191] used in many electronic and optoelectronic devices.[192 – 194] Coarse-crystalline samples are commonly employed electroluminophores, playing the same role in applied luminescence as played by silicon in semiconductor electronics. Owing to the unique combination of diverse morphology and physical and chemical properties, ZnS nanostructures have a broad range of practical applications.

The data presented in the review demonstrate that nanostructured zinc sulfide is synthesized by diverse methods; however, the kinetics and growth mechanism of these nanostructures are quite complex and are still not entirely clear. The desired properties of nanostructured ZnS can be achieved by means of synthesis providing controlled size and morphology and surface protection of the nanoparticles.

A specific feature of zinc sulfide is the small exciton radius $R_{ex} \approx 2.4 – 2.6$ nm. Zinc sulfide nanoparticles with $R_{ex} \leqslant 2.5$ nm, which could demonstrate quantum size effects such as a change in the band gap width, have been prepared by only a few authors (see, for example, Refs 48, 64 and 107). Due to the difficulty of synthesis of these nanoparticles, the properties of nanostructured zinc sulfide are mainly controlled by doping and by fabrication of multilayer composite nanostructures.

Analysis of published data indicates that composite materials based on zinc sulfide nanowires and doped quantum dots are most promising for many applications. Doped ZnS : Cu, ZnS : Mn and ZnS : Al nanocrystals are effective luminophores emitting in blue-green (~480 – 510 nm), orange (~590 – 630 nm) and blue (~480 – 500 nm) spectral ranges.

One may expect that further development of methods for the synthesis of ZnS nanoparticles of definite size and

specified shape would further expand the scope of their applicability in optoelectronics, biology and medicine.

In recent years, a considerable progress in the synthesis of nanostructured zinc sulfide has been made, but there are still some bottlenecks.

Stable colloid solutions contain the finest ($\sim$2 – 6 nm) ZnS nanoparticles, but their concentration is quite low. Therefore, a challenge is to obtain more concentrated colloid solutions that would retain long-term stability and small nanoparticle size.

Among the problems that have not been ultimately solved in the synthesis of nanostructured zinc sulfide, note the necessity to attain a narrow size distribution of the resulting nanoparticles and nanostructures. The synthesis of monodispersed nanoparticles and ZnS nanostructures is rather important, because their properties depend appreciably on their size and uniformity. Solving this problem is necessary for commercial production of high-quality materials and devices based on nanostructured zinc sulfide.

A key problem of the application of ZnS quantum dots in electronics is the necessity to fabricate large arrays of quantum dots with identical size and shape. Indeed, the synthesized quantum dots are usually arranged in a random manner on the substrate surface. For electronic applications, the prepared ZnS quantum dot arrays should be properly ordered, preferably *via* self-assembly, and should be compatible with optical devices and detectors. One more important problem arising in the use of ZnS quantum dot arrays is the decrease in the electrical conductivity in the presence of organic ligands.

Indeed, many authors noted that ZnS quantum dots and nanocrystals obtained from solutions possess poor conductivity due to the presence of an organic coating layer needed to control the quality and size distribution. Moreover, the coating (stabilizing) agents can decompose with time. In view of the above, an important challenge is to stabilize the nanocrystals in solutions without coating agents.

This review was written with the financial support of the Russian Science Foundation (Project No. 19-79-10101).

References

1. M.T.Sidot. *C. R. Acad. Sci.* (*Paris*), **63**, 188 (1866)
2. C.Fnondel, C.Palache. *Am. Miner.*, **35**, 29 (1950)
3. D.J.Chadi. *Annu. Rev. Mater. Sci.*, **24**, 45 (1994)
4. R.F.Brebrick. *J. Phys. Chem. Solids*, **4**, 190 (1958)
5. H.Fu, S.-W.Tsang. *Nanoscale*, **4**, 2187 (2012)
6. S.I.Sadovnikov, A.I.Gusev, A.A.Rempel. *Russ. Chem. Rev.*, **85**, 731 (2016)
7. Yu.A.Krutyakov, A.A.Kudrinskiy, A.Yu.Olenin, G.V.Lisichkin. *Russ. Chem. Rev.*, **77**, 233 (2008)
8. A.Tang, Yu.Wang, H.Ye, C.Zhou, C.Yang, X.Li, H.Peng, F.Zhang, Y.Hou, F.Teng. *Nanotechnology*, **24**, 355602 (2013)
9. C.Cui, X.Li, J.Liu, Y.Hou, Y.Zhao, G.Zhong. *Nanoscale Res. Lett.*, **10**, 43 (2015)
10. S.I.Sadovnikov, A.I.Gusev. *Eur. J. Inorg. Chem.*, 4944 (2016)
11. S.I.Sadovnikov, A.I.Gusev. *J. Mater. Chem., A*, **5**, 17676 (2017)
12. S.I.Sadovnikov, A.A.Rempel, A.I.Gusev. *Russ. Chem. Rev.*, **87**, 303 (2018)
13. S.Goel, F.Chen, W.Cai. *Small*, **10**, 631 (2013)
14. N.V.Hullavarad, S.S.Hullavarad, P.C.Karulkar. *J. Nanosci. Nanotechnol.*, **8**, 3272 (2008)
15. A.K.Mahapatra, A.K.Dash. *Physica E*, **35**, 9 (2006)
16. X.Wang, H.Huang, B.Liang, Z.Liu, D.Chen, G.Shen. *Crit. Rev. Solid State Mater. Sci.*, **38**, 57 (2013)
17. A.Shakil1, S.Das, A.Rahman, U.S.Akther, K.H.Majumdar, K.Rahman. *Mater. Sci. Appl.*, **9**, 751 (2018)
18. E.M.Gavrishchuk, E.V.Yashina. *Opt. Zh.*, (7), 56 (2005)
19. N.T.Gurin, A.V.Shlyapin, O.Yu.Sabitov. *Tech. Phys.*, **47**, 215 (2002)
20. G.Leftheriotis, S.Papaefthimiou, P.Yianoulis. *Sol. Energy Mater. Sol. Cells*, **61**, 107 (2000)
21. P.Hu, L.Bai, L.Yu, J.Li, F.Yuan, Y.Chen. *Nanoscale Res. Lett.*, **4**, 1047 (2009)
22. X.S.Fang, Y.Bando, C.H.Ye, G.Z.Shen, D.Golberg. *J. Phys. Chem, C* **111**, 8469 (2007)
23. C.H.Ye, Y.Bando, X.S.Fang, G.Z.Shen, D.Golberg. *J. Phys. Chem. C* **111**, 12673 (2007)
24. C.Ma, D.Moore, J.Li, Z.L.Wang. *Adv. Mater.*, **15**, 228 (2003)
25. R.B.Vasiliev, D.N.Dirin, A.M.Gaskov. *Russ. Chem. Rev.*, **80**, 1139 (2011)
26. R.C.Sharma, Y.A.Chang. *J. Phase Equil.*, **17**, 261 (1996)
27. J.T.S.Van Aswegen, H.Verleger. *Naturwissenschaften*, **47**, 131 (1960)
28. P.L.Smith, J.E.Martin. *Phys. Lett.*, **19**, 541 (1965)
29. E.H.Kisi, M.M.Elcombe. *Acta Crystallogr., Sect. C*, **45**, 1867 (1989)
30. K.Wright, G.W.Watson, S.C.Parker, D.J.Vaughan. *Am. Miner.*, **83**, 141 (1998)
31. V.-C.Lee, H-S.Wong. *Chin. J. Phys.*, **10**, 60 (1981)
32. S.-H.Na, C.-H.Park. *J. Korean Phys. Soc.*, **54**, 867 (2009)
33. D.Moore, Z.L.Wang. *J. Mater. Chem.*, **16**, 3898 (2006)
34. Z.Wang, L.L.Daemen, Y.Zhao, C.S.Zha, R.T.Down, X.Wang, Z.L.Wang, R.J.Hemley. *Nat. Mater.*, **4**, 922 (2005)
35. X.B.Jiang, B.B.Xiao, X.Y.Gu, X.H.Zhang. *Thin Solid Films*, **640**, 67 (2017)
36. M.Khalkhali, Q.Liu, H.Zeng, H.Zhang. *Sci. Rep.*, **5**, 14267 (2015)
37. M.Cardona, G.Harbeke. *Phys. Rev. A*, **137**, 1467 (1965)
38. *Landolt-Börnstein: Zahlenwerte und Funktionen aus Naturwissenschaften und Technik — Neue Serie/Grouppe III/41: Kristall- und Festkorperphysik. Bd 17b. Zinc Sulfide (ZnS) Energy Gap, Cubic Modification*. (Eds O.Madelung, U.Rössler, M.Schultz). (Berlin, Heidelberg, New York, Tokyo: Springer, 1999); https://materials.springer.com/lb/docs/sm_lbs_978-3-540-31359-5_315
39. J.C.Miklosz, R.G.Wheeler. *Phys. Rev.*, **153**, 913 (1967)
40. I.B.Kobyakov. *Kristallografiya*, **11**, 419 (1966)
41. I.B.Kobyakov,G.S.Pado. *Fiz. Tv. Tela*, **9**, 2173 (1967)
42. I.A.Dan'kov, I.B.Kobyakov, S.Yu.Davydov. *Fiz. Tv. Tela*, **24**, 3613 (1982)
43. A.I.Gusev, A.A.Rempel. *Nanocrystalline Materials*. (Cambridge: Cambridge Int. Sci. Publ., 2004)
44. A.I.Gusev. *Nanomaterialy, Nanostruktury, Nanotekhnologii*. (Nanomaterials, Nanostructures and Nanotechnologies). (Moscow: Fizmatlit, 2009)
45. H.-E.Schaefer. *Nanoscience. The Science of the Small in Physics, Engineering, Chemistry, Biology and Medicine*. (Heidelberg, Dordrecht, New York: Springer, 2010)
46. R.Rosetti, R.Hull, J.M.Gibson, L.E.Brus. *J. Chem. Phys.*, **82**, 552 (1985)
47. J.Joo, H.B.Na, T.Yu, J.H.Yu, Y.W.Kim, F.X.Wu, J.Z.Zhang, T.Hyeon. *J. Am. Chem. Soc.*, **125**, 11100 (2003)
48. Y.W.Zhao, Y.Zhang, H.Zhu, G.C.Hadjipanayis, J.Q.Xiao. *J. Am. Chem. Soc.*, **126**, 6874 (2004)

49. T.T.Q.Hoa, L.V.Vu, T.D.Canh, N.N.Long. *J. Phys.: Conf. Ser.*, **187**, 012081 (2009)
50. B.Bodo, R.Singh. *Int. J. Sci. Res. Publ.*, **6**, 461 (2016)
51. H.Zhang, S.Y.Zhang, S.Pan, G.P.Li, J.G.Hou. *Nanotechnology*, **15**, 945 (2004)
52. H.F.Shao, X.F.Qian, Z.K.Zhu. *J. Solid State Chem.*, **178**, 3522 (2005)
53. H.Zhou, T.X.Fan, D.Zhang, Q.X.Guo, H.Ogawa. *Chem. Mater.*, **19**, 2144 (2007)
54. S.Pal, B.Goswami, P.Sarkar. *J. Phys. Chem. C*, **112**, 6307 (2008)
55. N.Arul Dhas, A.Zaban, A.Gedanken. *Chem. Mater.*, **11**, 806 (1999)
56. J.L.Yin, X.F.Qian, J.Yin, M.W.Shi, G.T.Zhou. *Mater. Lett.*, **57**, 3859 (2003)
57. H.J.Liu, Y.H.Ni, M.Han, Q.Liu, Z.Xu, J.M.Hong, X.Ma. *Nanotechnology*, **16**, 2908 (2005)
58. Y.R.Ma, L.M.Qi, J.M.Ma, H.M.Cheng. *Langmuir*, **19**, 4040 (2003)
59. F.Gu, C.Z.Li, S.F.Wang, M.K.Lu. *Langmuir*, **22**, 1329 (2006)
60. Y.Y.Luo, G.T.Duan, M.Ye, Y.X.Zhang, G.H.Li. *J. Phys. Chem. C*, **112**, 2349 (2008)
61. H.Tong, Y.-J.Zhu, L.-X.Yang, L.Li, L.Zhang, J.Chang, L.-Q.An, S.-W.Wang. *J. Phys. Chem. C*, **111**, 3893 (2007)
62. D.V.Talapin, A.L.Rogach, A.Kornowski, M.Haase, H.Weller. *Nano Lett.*, **1**, 207 (2001)
63. R.G.Xie, U.Kolb, J.X.Li, T.Basche, A.Mews. *J. Am. Chem. Soc.*, **127**, 7480 (2005)
64. W.J.Zhang, G.J.Chen, J.Wang, B.-C.Ye, X.H.Zhong. *Inorg. Chem.*, **48**, 9723 (2009)
65. S.Biswas, T.Ghoshal, S.Kar, S.Chakrabarti, S.Chaudhuri. *Cryst. Growth. Des.*, **8**, 2171 (2008)
66. Y.W.Wang, L.D.Zhang, C.H.Liang, G.Z.Wang, X.S.Peng. *Chem. Phys. Lett.*, **357**, 314 (2002)
67. C.J.Barrelet, Y.Wu, D.C.Bell, C.M.Lieber. *J. Am. Chem. Soc.*, **125**, 11498 (2003)
68. C.Pacholski, A.Kornowski, H.Weller. *Angew. Chem., Int. Ed.*, **41**, 1188 (2002)
69. J.Yu, J.Joo, H.Û.Park, S.-I.Baik, Y.W.Kim, S.C.Kim, T.Hyeon. *J. Am. Chem. Soc.*, **127**, 5662 (2005)
70. G.Z.Shen, Y.Bando, D.Golberg, C.W.Zhou. *J. Phys. Chem. C*, **112**, 12299 (2008)
71. Y.C.Li, X.H.Li, C.H.Ye, Y.F.Li. *J. Phys. Chem. B*, **108**, 16002 (2004)
72. X.D.Wang, P.X.Gao, J.Li, C.J.Summers, Z.L.Wang. *Adv. Mater.*, **14**, 1732 (2002)
73. L.-W.Yin, Y.Bando, J.-H.Zhan, M.-S.Li, D.Golberg. *Adv. Mater.*, **17**, 1972 (2005)
74. X.Huang, M.-G.Willinger, H.Fan, Z.Xie, L.Wang, A.Klein-Hoffmann, F.Girgsdies, C.-S.Lee, X.-M.Meng. *Nanoscale*, **6**, 8787 (2014)
75. X.S.Fang, Y.Bando, M.Y.Liao, U.K.Gautam, C.Y.Zhi, B.Dierre, B.D.Liu, T.Y.Zhai, T.Sekiguchi, Y.Koide, D.Golberg. *Adv. Mater.*, **21**, 2034 (2009)
76. Y.Jiang, X.M.Meng, J.Liu, Z.Y.Xie, C.S.Lee, S.T.Lee. *Adv. Mater.*, **15**, 323 (2003)
77. J.Y.Li, Q.Zhang, L.An, L.C.Qin, J.Liu. *J. Solid State Chem.*, **181**, 3116 (2008)
78. X.S.Fang, Y.Bando, G.Z.Shen, C.H.Ye, U.K.Gautam, P.M.F.J.Costa. *Adv. Mater.*, **19**, 2593 (2007)
79. X.S.Fang, Y.Bando, C.H.Ye, D.Golberg. *Chem. Commun.*, **29**, 3048 (2007)
80. F.Lu, W.P.Cai, Y.G.Zhang, Y.Li, F.Q.Sun, S.H.Heo. *J. Phys. Chem. C*, **111**, 13385 (2007)
81. X.J.Wang, Q.L.Zhang, B.S.Zou, A.H.Lei, P.Y.Ren. *Appl. Surf. Sci.*, **257**, 10898 (2011)
82. S.L.Xiong, B.J.Xi, C.M.Wang, D.C.Xu, X.M.Feng, Z.C.Zhu, Y.T.Qian. *Adv. Funct. Mater.*, **17**, 2728 (2007)
83. Y.Xi, C.G.Hu, B.Feng, X.Wang, C.H.Zheng, X.S.He. *J. Supercond. Nov. Magn.*, **23**, 901 (2010)
84. J.Gong, S.Yang, H.Huang, J.Duan, H.Liu, X.Zhao, R.Zhang, Y.Du. *Small*, **2**, 732 (2006)
85. T.Y.Zhai, Y.Dong, Y.B.Wang, Z.W.Cao, Y.Ma, H.B.Fu, J.N.Yao. *J. Solid State Chem.*, **181**, 950 (2008)
86. Z.G.Chen, J.Zou, G.Liu, X.D.Yao, F.Li, X.L.Yuan. *Adv. Funct. Mater.*, **18**, 3063 (2008)
87. Y.F.Nicolau. *Appl. Surf. Sci.*, **22/23**, 1061 (1985)
88. Y.F.Nicolau, J.C.Menard. *J. Cryst. Growth*, **92**, 128 (1988)
89. Y.F.Nicolau, M.Dupuy, M.Brunel. *J. Electrochem. Soc.*, **137**, 2915 (1990)
90. A.Yoshikawa, S.Yamaga, K.Tanaka, H.Kasai. *J. Cryst. Growth*, **72**, 13 (1985)
91. I.P.McClean, C.B.Thomas. *Semicond. Sci. Technol.*, **7**, 1394 (1992)
92. J.M.Doña, J.Herrero. *J. Electrochem. Soc.*, **141**, 205 (1994)
93. L.Zhou, Y.Xue, J.Li. *J. Environm. Sci.*, **31** (Suppl.1), S76 (2009)
94. W.-L.Liu,W.-J.Chen, S.-H.Hsieh, J.-H.Yu. *Proc. Eng.*, **36**, 46 (2012)
95. S.M.Salim, A.H.Eid, A.M.Salem, H.M.Abou El-khair. *Surf. Interface Anal.*, **44**, 1214 (2012)
96. K.P.Murali, S.Vasantha, K.Rajamma. *Mater. Lett.*, **62**, 1823 (2008)
97. S.Lindroos, T.Kanniainen, M.Leskela. *Appl. Surf. Sci.*, **75**, 70 (1994)
98. R.Zhang, B.Wang, L.Wei. *Mater. Chem. Phys.*, **112**, 557 (2008)
99. D.H.Hwang, J.H.Ahn, K.N.Hui, K.S.Hui, Y.G.Son. *Nanoscale Res. Lett.*, **7**, 26 (2012)
100. T.Hurma. *J. Mol. Struct.*, **1161**, 279 (2018)
101. J.W.Cheon, D.S.Talaga, J.I.Zink. *J. Am. Chem. Soc.*, **119**, 163 (1997)
102. K.Ghezali, L.Mentar, B.Boudine, A.Azizi. *J. Electroanal. Chem.*, **794**, 212 (2017)
103. M.B.Dergacheva, K.A.Urazov, G.M.Khussurova, K.A.Leontyeva. *Coatings*, **6**, 14 (2016)
104. A.Wei, J.Liu, M.Zhuang, Y.Zhao. *Mater. Sci. Semicond. Proc.*, **16**, 1478 (2013)
105. J.S.Cruz, D.S.Cruz, M.C.Arenas-Arrocena, F.De Moure Flores, S.A.Mayén Hernández. *Chalcogen. Lett.*, **12**, 277 (2015)
106. J.P.Borah, K.C.Sarma. *Acta Phys. Polon. A*, **114**, 713 (2008)
107. R.Maity, K.K.Chattopadhyay. *Nanotechnology*, **15**, 812 (2004)
108. T.Kang, J.Sung, W.Shim, H.Moon, J.Cho, Y.Jo, W.Lee, B.Kim. *J. Phys. Chem. C*, **113**, 5352 (2009)
109. W.-L.Liu, C.-S.Yang, S.-H.Hsieh, W.-J.Chen, C.-L.Fern. *Appl. Surf. Sci.*, **264**, 213 (2013)
110. J.Ihanus, M.Ritala, M.Leskelä, T.Prohaska, R.Resch, G.Freidbacher. *Appl. Surf. Sci.*, **120**, 43 (1997)
111. A.Henglein. *Top. Curr. Chem.*, **143**, 113 (1988)
112. A.Henglein. *Chem. Rev.*, **89**, 1861 (1989)
113. Y.M.Tricot, J.H.Fendler. *J. Am. Chem. Soc.*, **106**, 7359 (1984)
114. M.Meyer, C.Wallberg, K.Kurihara, J.H.Fendler. *J. Chem. Soc., Chem. Commun.*, 90 (1984)
115. J.H.Fendler. *Chem. Rev.*, **87**, 877 (1987)
116. X.K.Zhao, S.Baral, R.Rolandi, J.H.Fendler. *J. Am. Chem. Soc.*, **110**, 1012 (1988)

117. Al.L.Efros, A.L.Efros. *Fiz. Tekh. Poluprovodnikov*, **16**, 1209 (1982)
118. A.I.Ekimov, A.A.Onushchenko. *Fiz. Tekh. Poluprovodnikov*, **16**, 1215 (1982)
119. A.I.Ekimov, A.A.Onushchenko. *JETP Lett.,* **40**, 1136 (1984)
120. L.E.Brus. *J. Chem. Phys.*, **79**, 5566 (1983)
121. L.E.Brus. *J. Chem. Phys.*, **80**, 4403 (1984)
122. R.Rosetti, R.Hull, J.M.Gibson, L.E.Brus. *J. Chem. Phys.*, **83**, 1406 (1985)
123. S.I.Sadovnikov, A.A.Rempel, A.I.Gusev. *Nanostructured Lead, Cadmium and Silver Sulfides: Structure, Nonstoichiometry and Properties*. (Cham, Heidelberg: Springer, 2018)
124. H.Weller, U.Koch, M.Gutierrez, A.Henglein. *Ber. Bunsenges. Phys. Chem.*, **88**, 649 (1984)
125. R.Rossetti, J.L.Ellison, J.M.Gibson, L.E.Brus. *J. Chem. Phys.*, **80**, 4464 (1984)
126. S.I.Sadovnikov, A.I.Gusev. *J. Alloys Compd.*, **586**, 105 (2014)
127. S.I.Sadovnikov, A.I.Gusev, A.A.Rempel. *Poluprovodnikovye Nanoctruktury Sul'fidov Svintsa, Cadmiya i Serebra*. (Semiconductor Nanostructures of Lead, Cadmium and Silver Sulfides). (Moscow: Fizmatlit, 2018)
128. L.Jing, S.V.Kershaw,Y.Li, X.Huang, Y.Li, A.L.Rogach, M.Gao. *Chem Rev.*, **116**, 10623 (2016)
129. G.A.Kitaev, I.T.Romanov. *Izv. Vyssh. Uchebn. Zaved., Khim. Khim. Tekhnol.*, **17**, 1427 (1974)
130. Yu.Yu.Lur'e. *Spravochnik po Analiticheskoi Khimii*. (Handbook of Analytical Chemistry). (Moscow: Khimiya, 1967)
131. P.Patnaik. *Dean's Analytical Chemistry Handbook*. (2nd Edn.). (New York: McGraw-Hill, 2004). Table 4.2
132. K.Hedayati, A.Zendehnam, F.Hassanpour. *J. Nanostruct.*, **6**, 207 (2016)
133. J.Zhang, J.Li, J.X.Zhang, R.G.Xie, W.S.Yang. *J. Phys. Chem. C*, **114**, 11087 (2010)
134. J.Q.Zhuang, X.D.Zhang, G.Wang, D.M.Li, W.S.Yang, T.J.Li. *J. Mater. Chem.*, **13**, 1853 (2003)
135. T.Akiyama, K.Sano, K.Nakamura, T.Ito. *Jpn. J. Appl. Phys.*, **46**, 1783 (2007)
136. X.Zhao, X.Ren, C.Sun, X.Zhang, Y.Si, C.Yan, J.Xu, D.Xue. *Funct. Mater. Lett.*, **1**, 167 (2008)
137. I.N.Stranski. *Bull. Soc. Fr. Min. Crist.*, **79**, 359 (1956)
138. M.Bienfait, R.Boistelle, R.Kern. *Adsorption et Croissance Cristalline*. (Paris: CNRS, 1965)
139. H.Z.Zhang, F.Huang, B.Gilbert, J.F.Banfield. *J. Phys. Chem., B,* **107**, 13051 (2003)
140. C.G.Lee, Y.Nakamura, H.Nakamura, M.Uehara, H.Maeda. *Építöanyag: J. Silic. Based Comp. Mater. (Hungary)*, **63**, 52 (2011); DOI: 10.14382/epitoanyag-jsbcm.2011.9
141. L.Wang, J.Dai, X.Liu, Z.Zhu, X.Huang, P.Wu. *Ceram. Int.*, **38**, 1873 (2012)
142. B.Ding, M.Shi, F.Chen, R.Zhou, M.Deng, M.Wang, H.Z.Chen. *J. Cryst. Growth*, **311**, 1533 (2009)
143. M.Shakouri-Arani, M.Salavati-Niasari. *J. Ind. Eng. Chem.*, **20**, 3141 (2014)
144. D.R.Frankle. *Phys. Rev.*, **111**, 1540 (1958)
145. P.Pipinys, A.Proskura, A.Rimeika. *Phys. Status Solidi*, **72**, 511 (1982)
146. E.Bringuier. *J. Appl. Phys.*, **75**, 291 (1994)
147. Y.I.Golovin, R.B.Morgunov, A.A.Baskakov, S.Z.Shmurak. *Phys. Solid State*, **41**, 1783 (1999)
148. T.Toyama, T.Hama, D.Adachi, Y.Nakashizu, H.Okamoto. *Nanotechnology*, **20**, 055203 (2009)
149. W.Chan, R.Sammynaiken, Y.Huang, J.O.Malm, R.Wallenberg, J.O.Bovin, V.Zwiller, N.A.Kotov. *J. Appl. Phys.*, **89**, 1120 (2001)
150. X.S.Fang, Y.Bando, D.Golberg. *J. Mater. Sci. Technol.*, **24**, 512 (2008)
151. T.Y.Zhai, Z.J.Gu, H.B.Fu, Y.Ma, J.N.Yao. *Cryst. Growth Des.*, **7**, 1388 (2007)
152. Y.C.Zhu, Y.Bando, D.F.Xue. *Appl. Phys. Lett.*, **82**, 1769 (2003)
153. X.S.Fang, C.H.Ye, L.D.Zhang, Y.H.Wang, Y.C.Wu. *Adv. Funct. Mater.*, **15**, 63 (2005)
154. Z.Li, B.Liu, X.Li, S.Yu, L.Wang, Y.Hou, Y.Zou, M.Yao, Q.Li, B.Zou, T.Cui, G.Zou, G.Wang, Y.Liu. *Nanotechnology*, **18**, 255602 (2007)
155. C.H.Zhou, H.Yuan, H.B.Shen, Y.Guo, X.M.Li, D.Liu, L.Xu, L.Ma, L.S.Li. *J. Mater. Chem.*, **21**, 7393 (2011)
156. J.J.Zheng, W.Y.Ji, X.Y.Wang, M.Ikezawa, P.T.Jing, X.Y.Liu, H.B.Li, J.L.Zhao, Y.Masumoto. *J. Phys. Chem. C*, **114**, 15331 (2010)
157. Q.H.Xiong, G.Chen, J.D.Acord, X.Liu, J.J.Zengel, H.R.Gutierrez, J.M.Redwing, L.C.Lew Yan Voon, B.Lassen, P.C.Eklund. *Nano. Lett.*, **4**, 1663 (2004)
158. B.Y.Geng, X.W.Liu, Q.B.Du, X.W.Wei, L.D.Zhang. *Appl. Phys. Lett.*, **88**, 163104 (2006)
159. N.Üzar, S.Okur, M.C.Arıkan. *Sens. Actuators, A*, **167**, 188 (2011)
160. P.Jiang, J.S.Jie, Y.Q.Yu, Z.Wang, C.Xie, X.W.Zhang, C.Y.Wu, L.Wang, Z.F.Zhu, L.B.Luo. *J. Mater. Chem.*, **22**, 6856 (2012)
161. Y.G.Liu, P.Feng, X.Y.Xue, S.L.Shi, X.Q.Fu, C.Wang, Y.G.Wang, T.H.Wang. *Appl. Phys. Lett.*, **90**, 042109 (2007)
162. Z.G.Chen, J.Zou, G.Liu, H.F.Lu, F.Li, G.Q.Lu, H.M.Cheng. *Nanotechnology*, **19**, 055710 (2008)
163. L.Luo, H.Chen, L.Zhang, K.Xu, Y.Lv. *Anal. Chim. Acta*, **635**, 183 (2009)
164. J.H.He, Y.Y.Zhang, J.Liu, D.Moore, G.Bao, Z.L.Wang. *J. Phys. Chem. C*, **111**, 12152 (2007)
165. M.Koneswaran, R.Narayanaswamy. *Sens. Actuators, B*, **139**, 104 (2009)
166. H.Li, C.Han. *Chem. Mater.*, **20**, 6053 (2008)
167. W.Luan, H.Yang, Z.Wan, B.Yuan, X.Yu, S.-T.Tu. *J. Nanopart. Res.*, **14**, 762 (2012)
168. R.Tu, B.Liu, Z.Wang, D.Gao, F.Wang, Q.Fang, Z.Zhang. *Anal. Chem.*, **80**, 3458 (2008)
169. H.D.Duong, J.Il.Rhee. *Talanta*, **73**, 899 (2007)
170. C.P.Huang, Y.K.Li, T.M.Chen. *Biosens. Bioelectron.*, **22**, 1835 (2007)
171. N.Verma, A.K.Singh, N.Saini. *Sensing Bio-sens. Res.*, **15**, 41 (2017)
172. S.Tarish, Y.Xu, Z.Wang, F.Mate, A.Al-Haddad, W.Wang, Y.Lei. *Nanotechnology*, **28**, 405501 (2017)
173. Y.Zhao, X.Wei, N.Peng, J.Wang, Z.Jiang. *Sensors*, **17**, 1235 (2017)
174. J.S.Hu, L.L.Ren, Y.G.Guo, H.P.Liang, A.M.Cao, L.J.Wan, C.L.Bai. *Angew. Chem., Int. Ed.*, **44**, 1269 (2005)
175. T.Nakada, M.Mitzutani. *Jpn. J. Appl. Phys.*, **41**, 165 (2002)
176. M.Bredol, M.Kaczmarek. *J. Phys. Chem. A*, **114**, 3950 (2010)
177. J.S.Steckel, P.Snee, S.Coe, J.P.Zimmer, J.E.Halpert, P.Anikeeva, L.Kim, V.Bulovic, M.G.Bawendi. *Angew. Chem., Int. Ed.*, **45**, 5796 (2006)
178. J.Lim, S.Jun, E.Jang, H.Baik, H.Kim, J.Cho. *Adv. Mater.*, **19**, 1927 (2007)
179. W.K.Bae, J.Kwak, J.W.Park, K.Char, C.Lee, S.Lee. *Adv. Mater.*, **21**, 1690 (2009)

180. E.Jang, S.Jun, H.Jang, J.Lim, B.Kim, Y.Kim. *Adv. Mater.*, **22**, 3076 (2010)
181. M.A.Hines, P.Guyot-Sionnest. *J. Phys. Chem.*, **100**, 468 (1996)
182. J.Chung, J.Myoung, J.Oh, S.Lim. *J. Phys. Chem.*, **114**, 21360 (2010)
183. X.-L.Yu, J.-G.Song, Y.-S.Fu, Y.Xie, X.Song, J.Sun, X.-W.Du. *J. Phys. Chem. C*, **114**, 2380 (2010)
184. N.Balis, V.Dracopoulos, K.Bourikas, P.Lianos. *Electrochim. Acta*, **91**, 246 (2013)
185. Y.N.Xia, P.D.Yang, Y.G.Sun, Y.U.Wu, B.Mayers, B.Gates, Y.Yin, F.Kim, H.Q.Yan. *Adv. Mater.*, **15**, 353 (2003)
186. *Semiconductor Nanostructures for Optoelectronic Applications*. (Ed. T.D.Steiner). (Boston, London: Artech House, 2004)
187. L.Yang, J.Han, T.Luo, M.Li, J.Huang, F.Meng. *Chem. – Asian J.*, **4**, 174 (2009)
188. N.K.Morozova, V.A.Kuznetsov. *Sul'fid Tsinka. Poluchenie i Opticheskie Svoistva*. (Zinc Sulfide. Preparation and Optical Properties). (Moscow: Nauka, 1987)
189. X.Fang, T.Zhai, U.K.Gautam, L.Li, L.Wu, Y.Bando, D.Golberg. *Prog. Mater. Sci.*, **56**, 175 (2011)
190. S.Ummartyotin, Y.Infahsaeng. *Renew. Sust. Energy Rev.*, **55**, 17 (2016)
191. N.Kaur, S.Kaur, J.Singh, M.Rawat. *J. Bioelectron. Nanotechnol.*, **1**, 1 (2016)
192. T.Kryshtab, V.S.Khomchenko, J.A.Andraca-Adame, A.K.Savin, A.Kryvko, G.Juárez, R.Peåa-Sierra. *J. Lumin.*, **129**, 1677 (2009)
193. X.Ma, J.Song, Z.Yu. *Thin Solid Films*, **519**, 5043 (2011)
194. M.D.A.Rahman, S.M.Said, S.Balamurugan. *Sci. Technol. Adv. Mater.*, **16**, 033501 (2015)